INTERNATIONAL JOURNAL FOR NUMERICAL METHODS IN ENGINEERING
*Int. J. Numer. Meth. Engng* (in press)
Published online in Wiley InterScience (www.interscience.wiley.com). DOI: 10.1002/nme.1282

# A FETI-DP method for the parallel iterative solution of indefinite and complex-valued solid and shell vibration problems

Charbel Farhat[1,*,†], Jing Li[2] and Philip Avery[1]

[1]*Department of Mechanical Engineering and Institute for Computational and Mathematical Engineering, Stanford University, Building 500, Stanford, CA 94305-3035, U.S.A.*
[2]*Department of Mathematical Sciences, Kent State University, Kent, OH 44242, U.S.A.*

SUMMARY

The dual-primal finite element tearing and interconnecting (FETI-DP) domain decomposition method (DDM) is extended to address the iterative solution of a class of indefinite problems of the form $(\mathbf{K}-\sigma^2\mathbf{M})\mathbf{u}=\mathbf{f}$, and a class of complex problems of the form $(\mathbf{K}-\sigma^2\mathbf{M}+\mathrm{i}\sigma\mathbf{D})\mathbf{u}=\mathbf{f}$, where $\mathbf{K}$, $\mathbf{M}$, and $\mathbf{D}$ are three real symmetric matrices arising from the finite element discretization of solid and shell dynamic problems, i is the imaginary complex number, and $\sigma$ is a real positive number. A key component of this extension is a new coarse problem based on the free-space solutions of Navier's equations of motion. These solutions are waves, and therefore the resulting DDM is reminiscent of the FETI-H method. For this reason, it is named here the FETI-DPH method. For a practically large $\sigma$ range, FETI-DPH is shown numerically to be scalable with respect to all of the problem size, substructure size, and number of substructures. The CPU performance of this iterative solver is illustrated on a 40-processor computing system with the parallel solution, for various $\sigma$ ranges, of several large-scale, indefinite, or complex-valued systems of equations associated with shifted eigenvalue and forced frequency response structural dynamics problems. Copyright © 2005 John Wiley & Sons, Ltd.

KEY WORDS: FETI-DP; FETI-DPH; domain decomposition; PCG; PGMRES; indefinite; complex

## 1. INTRODUCTION

Real linear or linearized systems of equations of the form

$$(\mathbf{K}-\sigma^2\mathbf{M})\mathbf{u}=\mathbf{f} \tag{1}$$

*Correspondence to: C. Farhat, Department of Aerospace Engineering Sciences and Center for Aerospace Structures, University of Colorado, Campus Box 429, Boulder, CO 80309-0429, U.S.A.
†E-mail: cfarhat@stanford.edu

Contract/grant sponsor: The Sandia National Laboratories; contract/grant number: 31095, 29341
Contract/grant sponsor: The National Science Foundation; contract/grant number: DMS-0209297

*Received 7 July 2004*
*Revised 27 August 2004*
*Accepted 3 November 2004*

and complex linear or linearized systems of equations of the form

$$\left(\mathbf{K} - \sigma^2\mathbf{M} + \mathrm{i}\sigma\mathbf{D}\right)\mathbf{u} = \mathbf{f} \tag{2}$$

are frequent in computational structural dynamics. Equation (1) is encountered, for example, in the finite element (FE) simulation of the forced response to a periodic excitation of an undamped mechanical system. In this case, $\mathbf{K}$ and $\mathbf{M}$ are the FE stiffness and mass matrices of the considered mechanical system, respectively, $\sigma$ is the circular frequency of the external periodic excitation, $\mathbf{f}$ is its amplitude, $\left(\mathbf{K} - \sigma^2\mathbf{M}\right)$ is the impedance of the mechanical system, and $\mathbf{u}$ is the amplitude of its forced response. Such problems also arise during the solution by an inverse shifted method [1] of the generalized symmetric eigenvalue problem $\mathbf{Ku} = \omega^2\mathbf{Mu}$ associated with an undamped mechanical system. In this example, $\mathbf{K}$ and $\mathbf{M}$ have the same meaning as in the previous case, $\left(\omega^2, \mathbf{u}\right)$ is a pair of eigenvalue and eigenvector representing the square of a natural circular frequency and the corresponding natural vibration mode of the undamped mechanical system, respectively, and the shift $\sigma^2$ is introduced to obtain quickly the closest eigenvalues to $\sigma^2$. In both examples given here, the matrix $\mathbf{K}$ is symmetric positive definite or semi-definite, $\mathbf{M}$ is symmetric positive definite, and therefore $\left(\mathbf{K} - \sigma^2\mathbf{M}\right)$ rapidly becomes indefinite when $\sigma$ is increased. Equation (2) is encountered in similar problems when the mechanical system is damped, in which case i denotes the pure imaginary number satisfying $\mathrm{i}^2 = -1$. $\mathbf{D}$ denotes the FE damping matrix and is assumed here to be symmetric positive definite.

With the pressing need for higher-fidelity, three-dimensional structural models with millions of degrees of freedom (dof), and the significant demands placed by direct methods on computer resources for storing and solving the associated large-scale linear and linearized systems of equations, a large segment of the computational structural mechanics community has shifted its attention from direct to iterative solution strategies. More specifically, domain decomposition-based preconditioned conjugate gradient (PCG) methods have emerged as powerful equation solvers in this field on both sequential and parallel computing platforms [2]. While most successful domain decomposition methods (DDMs) have been designed for the solution of symmetric positive (semi-) definite systems, some have targeted indefinite problems of the form given in (1) [3, 4]. The objective of this paper is to present an alternative DDM that addresses both classes of indefinite (Equation (1)) and complex (Equation (2)) problems, that is based on the FETI-DP [5, 6] DDM, and that is scalable when $\mathbf{K}$, $\mathbf{M}$, and $\mathbf{D}$ result from the FE discretization of solid, plate, and shell vibration problems. For this purpose, the remainder of this paper is organized as follows.

In Section 2, the dual-primal finite element tearing and interconnecting (FETI-DP) method is overviewed and its scalability properties are recalled. In Section 3, this DDM is extended to the solution of problems of the form given in Equations (1) and (2); this leads to the design of yet another iterative substructuring method named here the FETI-DPH method. Next, the relationship between problems (1) and (2) and Navier's displacement equations of motion is highlighted then exploited to construct an auxiliary coarse problem for accelerating the convergence of the FETI-DPH method. In Section 4, the parallel implementation of this DDM is briefly overviewed. In Section 5, its performance and scalability properties are demonstrated on a 40-processor Silicon Graphics system for several large-scale structural vibration problems featuring various $\sigma$ ranges. Finally, conclusions are offered in Section 6.

 

## 2. THE FETI-DP METHOD

The FETI-DP method [5, 6] is a third-generation FETI method (for example, see References [7–9]) developed for the scalable and fast iterative solution of systems of equations arising from the FE discretization of static, dynamic, second-order, and fourth-order elliptic partial differential equations (PDEs). When equipped with the Dirichlet preconditioner [10] and applied to plane stress/strain or shell problems, the condition number $\kappa$ of its interface problem grows asymptotically as [11]

$$\kappa = \mathcal{O}\left(1 + \log^2 \frac{H}{h}\right) \tag{3}$$

where $H$ and $h$ denote the substructure and mesh sizes, respectively. When equipped with the same Dirichlet preconditioner and an auxiliary coarse problem constructed by enforcing some set of optional constraints at the substructure interfaces [6], the condition number estimate (3) also holds for second-order scalar elliptic problems that model three-dimensional solid mechanics problems [12]. This estimate proves the numerical scalability of the FETI-DP method with respect to all of the problem size, substructure size, and number of substructures. More specifically, it suggests that one can expect FETI-DP to solve small-scale and large-scale problems in similar iteration counts (*numerical* scalability). This in turn suggests that when the FETI-DP method is well-implemented on a parallel processor, it should be capable of solving an $n$-times larger problem using an $n$-times larger number of processors in almost a constant CPU time (*parallel* scalability). This was demonstrated in practice for many complex structural mechanics problems (for example, see References [5, 6, 13] and the references cited therein).

In order to keep this paper as self-contained as possible, the FETI-DP method is next overviewed in the context of the generic symmetric positive semi-definite static problem

$$\mathbf{Ku} = \mathbf{f} \tag{4}$$

where $\mathbf{K}$ has the same meaning as in problems (1) and (2), and $\mathbf{f}$ is an arbitrary load vector.

### 2.1. Substructuring and notation

Let $\Omega$ denote the computational support of a solid mechanics or shell problem whose discretization leads to problem (4), $\{\Omega^{(s)}\}_{s=1}^{N_s}$ denote its decomposition into $N_s$ substructures with matching interfaces $\Gamma^{(s,q)} = \partial\Omega^{(s)} \cap \partial\Omega^{(q)}$, and let $\Gamma = \bigcup_{s=1,q>s}^{s=N_s} \Gamma^{(s,q)}$ denote the global interface of this decomposition. *In the remainder of this paper, each interface* $\Gamma^{(s,q)}$ *is referred to as an* '*edge*', *whether* $\Omega$ *is a two- or three-dimensional domain*. Let also $\mathbf{K}^{(s)}$ and $\mathbf{f}^{(s)}$ denote the contributions of substructure $\Omega^{(s)}$ to $\mathbf{K}$ and $\mathbf{f}$, respectively, and let $\mathbf{u}^{(s)}$ denote the vector of dof associated with it.

Let $N_c$ of the $N_I$ nodes lying on the global interface $\Gamma$ be labelled 'corner' nodes (see Figure 1), $\Gamma_c$ denote the set of these corner nodes, and let $\Gamma' = \Gamma \backslash \Gamma_c$. The selection of the corner nodes is briefly discussed in Section 2.3. If in each substructure $\Omega^{(s)}$ the unknowns are partitioned into global corner dof designated by the subscript c, and 'remaining' dof designated

 

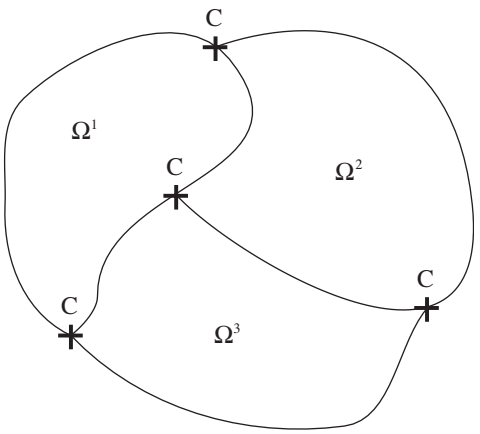


Figure 1. Example of a definition of corner points.

by the subscript r, $\mathbf{K}^{(s)}$, $\mathbf{u}^{(s)}$ and $\mathbf{f}^{(s)}$ can be partitioned as follows:

$$\mathbf{K}^{(s)} = \begin{bmatrix} \mathbf{K}_{\mathrm{rr}}^{(s)} & \mathbf{K}_{\mathrm{rc}}^{(s)} \\ \mathbf{K}_{\mathrm{rc}}^{(s)^{\mathrm{T}}} & \mathbf{K}_{\mathrm{cc}}^{(s)} \end{bmatrix}, \quad \mathbf{u}^{(s)} = \begin{bmatrix} \mathbf{u}_{\mathrm{r}}^{(s)} \\ \mathbf{u}_{\mathrm{c}}^{(s)} \end{bmatrix} \quad \text{and} \quad \mathbf{f}^{(s)} = \begin{bmatrix} \mathbf{f}_{\mathrm{r}}^{(s)} \\ \mathbf{f}_{\mathrm{c}}^{(s)} \end{bmatrix} \tag{5}$$

The r-type dof can be further partitioned into 'interior' dof designated by the subscript i, and substructure interface 'boundary' dof designated by the subscript b. Hence, $\mathbf{u}_{\mathrm{r}}^{(s)}$ and $\mathbf{f}_{\mathrm{r}}^{(s)}$ can be further partitioned as follows:

$$\mathbf{u}_{\mathrm{r}}^{(s)} = \begin{bmatrix} \mathbf{u}_{\mathrm{i}}^{(s)} & \mathbf{u}_{\mathrm{b}}^{(s)} \end{bmatrix}^{\mathrm{T}} \quad \text{and} \quad \mathbf{f}_{\mathrm{r}}^{(s)} = \begin{bmatrix} \mathbf{f}_{\mathrm{i}}^{(s)} & \mathbf{f}_{\mathrm{b}}^{(s)} \end{bmatrix}^{\mathrm{T}} \tag{6}$$

where the superscript T designates the transpose.

Let $\mathbf{u}_{\mathrm{c}}$ denote the global vector of corner dof, and $\mathbf{u}_{\mathrm{c}}^{(s)}$ denote its restriction to $\Omega^{(s)}$. Let also $\mathbf{B}_{\mathrm{r}}^{(s)}$ and $\mathbf{B}_{\mathrm{c}}^{(s)}$ be the two substructure Boolean matrices defined by

$$\mathbf{B}_{\mathrm{r}}^{(s)}\mathbf{u}_{\mathrm{r}}^{(s)} = \pm\,\mathbf{u}_{\mathrm{b}}^{(s)} \quad \text{and} \quad \mathbf{B}_{\mathrm{c}}^{(s)}\mathbf{u}_{\mathrm{c}} = \mathbf{u}_{\mathrm{c}}^{(s)} \tag{7}$$

where the $\pm$ sign is set by any convention that implies that $\sum_{s=1}^{N_s} \mathbf{B}_{\mathrm{r}}^{(s)}\mathbf{u}_{\mathrm{r}}^{(s)}$ represents the *jump* of the displacement solution $\mathbf{u}$ across the substructure interfaces. Finally, let

$$\mathbf{f}_{\mathrm{c}} = \sum_{s=1}^{N_s} \mathbf{B}_{\mathrm{c}}^{(s)^{\mathrm{T}}}\mathbf{f}_{\mathrm{c}}^{(s)} \tag{8}$$

In References [5, 6], it was shown that solving problem (4) is equivalent to solving the following substructure-based problems:

$$\mathbf{K}_{\mathrm{rr}}^{(s)}\mathbf{u}_{\mathrm{r}}^{(s)} + \mathbf{K}_{\mathrm{rc}}^{(s)}\mathbf{B}_{\mathrm{c}}^{(s)}\mathbf{u}_{\mathrm{c}} + \mathbf{B}_{\mathrm{r}}^{(s)^{\mathrm{T}}}\lambda + \mathbf{B}_{\mathrm{r}}^{(s)^{\mathrm{T}}}\mathbf{Q}_{\mathrm{b}}\boldsymbol{\mu} = \mathbf{f}_{\mathrm{r}}^{(s)}, \quad s = 1, \ldots, N_s \tag{9}$$

 

$$\sum_{s=1}^{N_s} \mathbf{B}_{\mathrm{c}}^{(s)^{\mathrm{T}}} \mathbf{K}_{\mathrm{rc}}^{(s)^{\mathrm{T}}} \mathbf{u}_{\mathrm{r}}^{(s)} + \sum_{s=1}^{N_s} \mathbf{B}_{\mathrm{c}}^{(s)^{\mathrm{T}}} \mathbf{K}_{\mathrm{cc}}^{(s)} \mathbf{B}_{\mathrm{c}}^{(s)} \mathbf{u}_{\mathrm{c}} = \mathbf{f}_{\mathrm{c}} \tag{10}$$

$$\sum_{s=1}^{N_s} \mathbf{B}_{\mathrm{r}}^{(s)} \mathbf{u}_{\mathrm{r}}^{(s)} = 0 \tag{11}$$

$$\mathbf{Q}_{\mathrm{b}}^{\mathrm{T}} \sum_{s=1}^{N_s} \mathbf{B}_{\mathrm{r}}^{(s)} \mathbf{u}_{\mathrm{r}}^{(s)} = 0 \tag{12}$$

where $\lambda$ is an $N_\lambda$-long vector of Lagrange multipliers introduced on $\Gamma'$ to enforce the continuity (11) of the displacement vector $\mathbf{u}$, and $\boldsymbol{\mu}$ is another vector of Lagrange multipliers introduced to enforce the optional linear constraints (12). These optional constraints, a concept first developed in Reference [14], generate a matrix $\mathbf{Q}_{\mathrm{b}}$ with $N_Q < N_\lambda$ columns defined on $\Gamma'$. The word 'optional' refers to the fact that Equation (12) and the vector of Lagrange multipliers $\boldsymbol{\mu}$ are not necessarily needed for formulating the above substructure-based problem. Indeed, since the solution of problem (4) is continuous across the substructure interfaces, it satisfies Equation (11) and therefore satisfies Equation (12) for any matrix $\mathbf{Q}_{\mathrm{b}}$. Note also that each of Equations (9) is a local substructure equation, whereas Equation (10) is an assembled global equation.

The substructure-based problem (9)–(12) was labelled 'dual-primal' in References [5, 6] because it is formulated in terms of two different types of global unknowns: the dual Lagrange multipliers represented by the vector $\lambda$, and the primal corner dof represented by the vector $\mathbf{u}_{\mathrm{c}}$.

In the remainder of this paper, the $j$th column of $\mathbf{Q}_{\mathrm{b}}$ is denoted by $\mathbf{q}_j$ so that

$$\mathbf{Q}_{\mathrm{b}} = \begin{bmatrix} \mathbf{q}_1 & \cdots & \mathbf{q}_j & \cdots & \mathbf{q}_{N_Q} \end{bmatrix} \tag{13}$$

### *2.2. Interface and coarse problems*

Let

$$\widetilde{\mathbf{K}}_{\mathrm{cc}} = \begin{bmatrix} \mathbf{K}_{\mathrm{cc}} & 0 \\ 0 & 0 \end{bmatrix}, \quad \mathbf{K}_{\mathrm{cc}} = \sum_{s=1}^{N_s} \mathbf{B}_{\mathrm{c}}^{(s)^{\mathrm{T}}} \mathbf{K}_{\mathrm{cc}}^{(s)} \mathbf{B}_{\mathrm{c}}^{(s)}, \quad \mathbf{d}_{\mathrm{r}} = \sum_{s=1}^{N_s} \mathbf{B}_{\mathrm{r}}^{(s)} \mathbf{K}_{\mathrm{rr}}^{(s)^{-1}} \mathbf{f}_{\mathrm{r}}^{(s)}$$

$$\text{and} \quad \mathbf{f}_{\mathrm{c}}^{*} = \mathbf{f}_{\mathrm{c}} - \sum_{s=1}^{N_s} \left( \mathbf{K}_{\mathrm{rc}}^{(s)} \mathbf{B}_{\mathrm{c}}^{(s)} \right)^{\mathrm{T}} \mathbf{K}_{\mathrm{rr}}^{(s)^{-1}} \mathbf{f}_{\mathrm{r}}^{(s)} \tag{14}$$

After some algebraic manipulations aimed at eliminating $\mathbf{u}_{\mathrm{r}}^{(s)}$, $s = 1, \ldots, N_s$, $\mathbf{u}_{\mathrm{c}}$, and $\mu$, the substructure-based problem (9)–(12) can be transformed into the following symmetric positive semi-definite interface problem:

$$\left( \mathbf{F}_{I_{\mathrm{rr}}} + \widetilde{\mathbf{F}}_{I_{\mathrm{rc}}} \widetilde{\mathbf{K}}_{\mathrm{cc}}^{*^{-1}} \widetilde{\mathbf{F}}_{I_{\mathrm{rc}}}^{\mathrm{T}} \right) \lambda = \mathbf{d}_{\mathrm{r}} - \widetilde{\mathbf{F}}_{I_{\mathrm{rc}}} \widetilde{\mathbf{K}}_{\mathrm{cc}}^{*^{-1}} \tilde{\mathbf{f}}_{\mathrm{c}}^{*} \tag{15}$$

where

$$\mathbf{F}_{I_{\mathrm{rr}}} = \sum_{s=1}^{N_s} \mathbf{B}_{\mathrm{r}}^{(s)} \mathbf{K}_{\mathrm{rr}}^{(s)^{-1}} \mathbf{B}_{\mathrm{r}}^{(s)^{\mathrm{T}}}, \quad \widetilde{\mathbf{F}}_{I_{\mathrm{rc}}} = \sum_{s=1}^{N_s} \mathbf{B}_{\mathrm{r}}^{(s)} \mathbf{K}_{\mathrm{rr}}^{(s)^{-1}} \widetilde{\mathbf{K}}_{\mathrm{rc}}^{(s)}$$

 

$$\widetilde{\mathbf{K}}_{\mathrm{rc}}^{(s)} = \left[\mathbf{K}_{\mathrm{rc}}^{(s)}\mathbf{B}_{\mathrm{c}}^{(s)} \;\; \mathbf{B}_{\mathrm{r}}^{(s)\mathrm{T}}\mathbf{Q}_{\mathrm{b}}\right], \quad \tilde{\mathbf{f}}_{\mathrm{c}}^{*} = \begin{bmatrix} \mathbf{f}_{\mathrm{c}}^{*} \\ -\mathbf{Q}_{\mathrm{b}}^{\mathrm{T}}\mathbf{d}_{\mathrm{r}} \end{bmatrix}$$

$$\widetilde{\mathbf{K}}_{\mathrm{cc}}^{*} = \widetilde{\mathbf{K}}_{\mathrm{cc}} - \begin{bmatrix} \sum_{s=1}^{N_s}\left(\mathbf{K}_{\mathrm{rc}}^{(s)}\mathbf{B}_{\mathrm{c}}^{(s)}\right)^{\mathrm{T}}\mathbf{K}_{\mathrm{rr}}^{(s)^{-1}}\left(\mathbf{K}_{\mathrm{rc}}^{(s)}\mathbf{B}_{\mathrm{c}}^{(s)}\right) & \sum_{s=1}^{N_s}\left(\mathbf{K}_{\mathrm{rc}}^{(s)}\mathbf{B}_{\mathrm{c}}^{(s)}\right)^{\mathrm{T}}\mathbf{K}_{\mathrm{rr}}^{(s)^{-1}}\left(\mathbf{B}_{\mathrm{r}}^{(s)\mathrm{T}}\mathbf{Q}_{\mathrm{b}}\right) \\ \sum_{s=1}^{N_s}\left(\mathbf{B}_{\mathrm{r}}^{(s)\mathrm{T}}\mathbf{Q}_{\mathrm{b}}\right)^{\mathrm{T}}\mathbf{K}_{\mathrm{rr}}^{(s)^{-1}}\left(\mathbf{K}_{\mathrm{rc}}^{(s)}\mathbf{B}_{\mathrm{c}}^{(s)}\right) & \sum_{s=1}^{N_s}\left(\mathbf{B}_{\mathrm{r}}^{(s)\mathrm{T}}\mathbf{Q}_{\mathrm{b}}\right)^{\mathrm{T}}\mathbf{K}_{\mathrm{rr}}^{(s)^{-1}}\left(\mathbf{B}_{\mathrm{r}}^{(s)\mathrm{T}}\mathbf{Q}_{\mathrm{b}}\right) \end{bmatrix} \tag{16}$$

The FETI-DP method is a DDM that solves the original problem (4) by applying a PCG algorithm to the solution of the corresponding dual interface problem (15). At the $n$th PCG iteration, the matrix–vector product $\left(\mathbf{F}_{I_{\mathrm{rr}}} + \widetilde{\mathbf{F}}_{I_{\mathrm{rc}}}\widetilde{\mathbf{K}}_{\mathrm{cc}}^{*^{-1}}\widetilde{\mathbf{F}}_{I_{\mathrm{rc}}}^{\mathrm{T}}\right)\lambda^n$ incurs the solution of an auxiliary problem of the form

$$\widetilde{\mathbf{K}}_{\mathrm{cc}}^{*}\mathbf{z} = \widetilde{\mathbf{F}}_{I_{\mathrm{rc}}}^{\mathrm{T}}\lambda^n \tag{17}$$

From the fifth of Equations (16), it follows that the size of this auxiliary problem is equal to the sum of the number of corner dof, $N_{\mathrm{c}}^{\mathrm{dof}}$, and the number of columns of the matrix $\mathbf{Q}_{\mathrm{b}}$, $N_Q$.

For $N_Q = 0$—that is, for $\mathbf{Q}_{\mathrm{b}} = 0$, the auxiliary problem (17) is a coarse problem, and $\widetilde{\mathbf{K}}_{\mathrm{cc}}^{*}$ is a sparse matrix whose pattern is that of the stiffness matrix obtained when each substructure is treated as a 'superelement' whose nodes are its corner nodes. This coarse problem ensures that the FETI-DP method equipped with the Dirichlet preconditioner (see Section 2.4) is numerically scalable for plate and shell problems as well as two-dimensional plane stress/strain problems [6, 11]. However, for $\mathbf{Q}_{\mathrm{b}} = 0$, the FETI-DP method equipped with the Dirichlet preconditioner is not numerically scalable for three-dimensional solid problems.

For any choice of $\mathbf{Q}_{\mathrm{b}} \neq 0$, $\widetilde{\mathbf{K}}_{\mathrm{cc}}^{*}$ remains a sparse matrix. If $\mathbf{Q}_{\mathrm{b}}$ is constructed edgewise—that is, if each column of $\mathbf{Q}_{\mathrm{b}}$ is constructed as the restriction of some operator to a specific edge of $\Gamma'$—the sparsity pattern of $\widetilde{\mathbf{K}}_{\mathrm{cc}}^{*}$ becomes that of a stiffness matrix obtained by treating each substructure as a superelement whose nodes are its corner nodes augmented by virtual mid-side nodes. The number of dof attached to each virtual mid-side node is equal to the number of columns of $\mathbf{Q}_{\mathrm{b}}$ associated with the edge on which lies this mid-side node. If $N_Q$ is kept relatively small, the auxiliary problem (17) remains a relatively small coarse problem. This coarse problem was labelled 'augmented' coarse problem in Reference [5] in order to distinguish it from the smaller coarse problem obtained with $\mathbf{Q}_{\mathrm{b}} = 0$. Furthermore, each column of $\mathbf{Q}_{\mathrm{b}}$ is referred to as an 'augmentation coarse mode'. When these augmentation coarse modes are chosen as the translational rigid body modes of each edge of $\Gamma'$, each three consecutive columns of $\mathbf{Q}_{\mathrm{b}}$ can be written as follows:

$$\begin{aligned} \mathbf{q}_x &= [0 \;\cdots\; 0 \;[1\;0\;0 \;\cdots\; 1\;0\;0 \;\cdots\; 1\;0\;0]\; 0 \;\cdots\; 0]^{\mathrm{T}} \\ \mathbf{q}_y &= [0 \;\cdots\; 0 \;[0\;1\;0 \;\cdots\; 0\;1\;0 \;\cdots\; 0\;1\;0]\; 0 \;\cdots\; 0]^{\mathrm{T}} \\ \mathbf{q}_z &= [0 \;\cdots\; 0 \;[0\;0\;1 \;\cdots\; 0\;0\;1 \;\cdots\; 0\;0\;1]\; 0 \;\cdots\; 0]^{\mathrm{T}} \end{aligned} \tag{18}$$

and the FETI-DP method equipped with the Dirichlet preconditioner becomes numerically scalable for three-dimensional scalar elliptic problems [12]. In (18), each of the vectors

 

$\mathbf{q}_x$, $\mathbf{q}_y$, and $\mathbf{q}_z$ has non-zero entries only between the pair of brackets [ ] delimiting the dof attached to the edge associated with these three vectors. Within these brackets, the sequence 1 0 0 corresponds to a translational rigid body mode of this edge in the $x$-direction, the sequence 0 1 0 corresponds to a translational rigid body mode in the $y$-direction, and the sequence 0 0 1 corresponds to a translational rigid body mode in the $z$-direction.

### 2.3. Corner selection

From the definitions of $\mathbf{F}_{I_{\mathrm{rr}}}$, $\widetilde{\mathbf{K}}^*_{\mathrm{cc}}$, and $\mathbf{d}_{\mathrm{r}}$ given in (16), (14) it follows that the corner nodes must be chosen such that $\mathbf{K}^{(s)}_{\mathrm{rr}}$ is non-singular. From Equation (15), it follows that when $\mathbf{Q}_{\mathrm{b}} \neq 0$, the selection of the corner nodes must furthermore guarantee that $\widetilde{\mathbf{K}}^*_{\mathrm{cc}}$ is non-singular. From the theory and results exposed in References [15, 16], it follows that the corner nodes must also include crosspoints—that is, points that belong to three or more substructures—when these are attached to a beam, plate, or shell element. A corner selection algorithm that meets all of these requirements was proposed and discussed in Reference [17].

### 2.4. Local preconditioning

So far, two local preconditioners, originally developed for the FETI method, have been applied with the FETI-DP approach:

1. The Dirichlet preconditioner which can be written as

$$\overline{\mathbf{F}}^{D^{-1}}_{I_{\mathrm{rr}}} = \sum_{s=1}^{N_s} \mathbf{W}^{(s)} \mathbf{B}^{(s)}_{\mathrm{r}} \begin{bmatrix} 0 & 0 \\ 0 & \mathbf{S}^{(s)}_{\mathrm{bb}} \end{bmatrix} \mathbf{B}^{(s)^{\mathrm{T}}}_{\mathrm{r}} \mathbf{W}^{(s)}$$

   where

$$\mathbf{S}^{(s)}_{\mathrm{bb}} = \mathbf{K}^{(s)}_{\mathrm{bb}} - \mathbf{K}^{(s)^{\mathrm{T}}}_{\mathrm{ib}} \mathbf{K}^{(s)^{-1}}_{\mathrm{ii}} \mathbf{K}^{(s)}_{\mathrm{ib}} \tag{19}$$

   the subscripts i and b have the same meaning as in Section 2.1, and $\mathbf{W}^{(s)}$ is a substructure diagonal scaling matrix that accounts for possible substructure heterogeneities [18]. The roots of this preconditioner and its mechanical interpretation can be found in Reference [10]. It is mathematically optimal in the sense that it leads to the condition number estimate (3).
2. The lumped preconditioner which can be written as

$$\overline{\mathbf{F}}^{L^{-1}}_{I_{\mathrm{rr}}} = \sum_{s=1}^{N_s} \mathbf{W}^{(s)} \mathbf{B}^{(s)}_{\mathrm{r}} \begin{bmatrix} 0 & 0 \\ 0 & \mathbf{K}^{(s)}_{\mathrm{bb}} \end{bmatrix} \mathbf{B}^{(s)^{\mathrm{T}}}_{\mathrm{r}} \mathbf{W}^{(s)} \tag{20}$$

   The roots of this preconditioner and its mechanical interpretation can be found in Reference [8]. This preconditioner is not mathematically optimal in the sense defined above; however, it decreases the cost of each iteration in comparison with the Dirichlet preconditioner often with a modest increase in the iteration count.

The Dirichlet preconditioner is less economical per iteration than the lumped preconditioner. However, experience has shown that it is more computationally efficient when $\mathbf{K}$ in problem (4) arises from the discretization of shell problems. When $\mathbf{K}$ arises from plane stress/strain and

 

solid mechanics problems, the lumped preconditioner becomes more computationally efficient even though it is not mathematically optimal.

## 3. THE FETI-DPH METHOD

Let

$$\mathbf{Z} = \mathbf{K} - \sigma^2 \mathbf{M} \tag{21}$$

$$\mathbf{Z}_{rr}^{(s)} = \mathbf{K}_{rr}^{(s)} - \sigma^2 \mathbf{M}_{rr}^{(s)} \tag{22}$$

and

$$\mathbf{Z}_{rr}^{D(s)} = \mathbf{K}_{rr}^{(s)} - \sigma^2 \mathbf{M}_{rr}^{(s)} + \mathrm{i}\sigma \mathbf{D}_{rr}^{(s)} \tag{23}$$

In the context of Equations (1) and (2), $\mathbf{Z}_{rr}^{(s)}$ and $\mathbf{Z}_{rr}^{D(s)}$, respectively, replace $\mathbf{K}_{rr}^{(s)}$ in the formulation of the FETI-DP method. Hence, the direct application of this DDM to the solution of problem (1) or (2) raises the following questions:

1. For the aforementioned applications and in the absence of damping, most $\sigma^2$ values of practical interest cause the global impedance matrix $\mathbf{Z}$ to be indefinite. In this case, are the substructure matrices $\mathbf{Z}_{rr}^{(s)}$ also indefinite? Furthermore, can any of these substructure impedances become singular or nearly singular?
2. In the context of Equation (2), the dual interface problem (15) is complex-valued. What is its type (positive definite or indefinite) in the context of real-valued problems of the form given in (1)?
3. The augmentation coarse modes (18) address neither the physical nor the mathematical nature of problem (1) or (2). Which augmentation coarse modes do?

The significance of the above three questions can be summarized as follows.

The answer to the first question impacts the solution of the local substructure problems (9). For a given $\sigma^2$, it is very difficult to determine in practice (finite arithmetic) whether a substructure impedance matrix $\mathbf{Z}_{rr}^{(s)}$ is singular or not. However, $\mathbf{Z}_{rr}^{(s)}$ is very ill-conditioned when $\sigma^2$ coincides with or is very close to an eigenvalue of the pencil $\left(\mathbf{K}_{rr}^{(s)}, \mathbf{M}_{rr}^{(s)}\right)$. This can be alarming because round-off errors are known to give rise to erroneous solutions to very ill-conditioned problems. It should also be noted that FETI-DP as well as most DDMs rely on a direct method for solving the local substructure problems. In the event of an indefinite impedance matrix $\mathbf{Z}_{rr}^{(s)}$, the performance of a direct skyline or sparse solver significantly degrades because pivoting becomes required. This in turn can degrade the CPU performance of a DDM.

The objective of the second question is to determine the Krylov method that is most suitable for solving the dual interface problem (15).

The third question aims at recognizing that for structural dynamics applications, there are perhaps other important modes besides the substructure rigid body modes that can accelerate the iterative solution of the dual interface problem (15).

Next, the three questions raised above are addressed in some detail, and the Dirichlet and lumped preconditioners summarized in Section 2.4 are tailored to the target applications of this

 

paper. This leads to the development of yet another FETI method, named here the FETI-DPH method, for the parallel iterative solution of problems (1) and (2).

### *3.1. On the type of the local undamped substructure problems*

Even in the context of Equation (1) (and for that matter also Equation (2)), the corner nodes selected by the FETI-DP solver are such that each substructure matrix $\mathbf{K}_{rr}^{(s)}$ is non-singular. However, at least in theory, $\mathbf{Z}_{rr}^{(s)}$ will still be singular when $\sigma^2$ coincides with an eigenvalue of the pencil $\left(\mathbf{K}_{rr}^{(s)}, \mathbf{M}_{rr}^{(s)}\right)$. This issue was addressed in Reference [19] in the context of the basic FETI method [7, 8] and acoustic scattering applications—that is, for the scalar exterior Helmholtz problem where $\sigma^2 = k^2$ and $k$ denotes the wave number. More specifically, a regularization procedure was developed in [19] to prevent all substructure problems from being singular for any value of the wave number $k$, without destroying the sparsity of the local matrices $\mathbf{K}_{rr}^{(s)} - k^2\mathbf{M}_{rr}^{(s)}$ and without affecting the solution of the original problem (1). The resulting DDM was named the FETI-H method (H for Helmholtz). Unfortunately, the regularization procedure characterizing the FETI-H method transforms each real-valued substructure problem associated with Equation (1) into a complex-valued substructure problem. For acoustic scattering applications, this is not an issue because the Sommerfeld radiation condition causes the solution of the original problem to be complex-valued. However, for real-valued problems such as those represented by Equation (1), the regularization procedure of the FETI-H method is unjustifiable from both computational resource and performance viewpoints. For this reason, a different approach is adopted here for addressing the type and potential singularity of a local substructure matrix $\mathbf{Z}_{rr}^{(s)}$.

In practice, if $\sigma$ approaches a natural circular frequency of the structure or coincides with it, $\mathbf{Z}_{rr}^{(s)}$ becomes only very ill-conditioned because of the effect of finite arithmetic. Therefore, two interesting questions are:

1. What are the odds that a given $\sigma^2$ of *practical interest* coincides with an eigenvalue of the pencil $\left(\mathbf{K}_{rr}^{(s)}, \mathbf{M}_{rr}^{(s)}\right)$?
2. For a given $\sigma^2$, can anything *reasonable* be done to prevent $\mathbf{Z}_{rr}^{(s)}$ from being singular or very ill-conditioned?

To address the above two questions, the $a \times a$ square plate shown in Figure 2 is considered. This plate is assumed to be simply supported on its four edges. Therefore, its natural circular frequencies are given by Géradin and Rixen [20]

$$\omega_{rn} = \frac{\pi^2}{a^2}\left(r^2 + n^2\right)\sqrt{\frac{D}{m}}, \quad r, n = 1, 2, \ldots, \infty \tag{24}$$

where

$$m = \rho\tau, \quad D = \frac{E\tau^3}{12\left(1 - \nu^2\right)} \tag{25}$$

$\rho$ and $\tau$ denote, respectively, the density and thickness of the plate and therefore $m$ denotes its mass per unit area, and $E$ and $\nu$ denote its Young modulus and Poisson coefficient, respectively.

Next, suppose that this plate is decomposed into $\sqrt{N_s} \times \sqrt{N_s}$ substructures (Figure 2). In this case, each substructure is a square of size $a/\sqrt{N_s}$. In the FETI-DP method, each

 

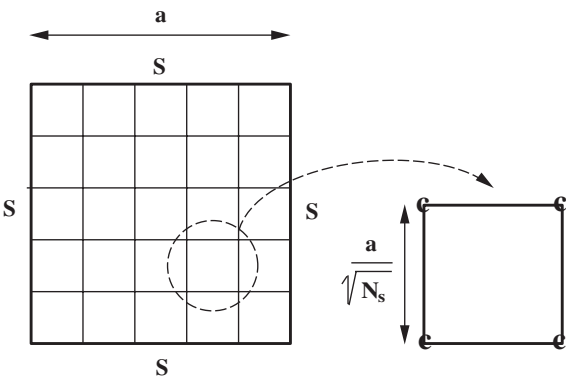


Figure 2. Square plate simply supported on its four edges—decomposition into $N_s$ uniform substructures.

substructure away from the boundary conditions is supported at its four corner nodes (see Figure 2) (more precisely, the transverse displacement as well as the rotation dof are fixed at the corner nodes). Hence, the natural circular frequency of the first vibration mode of such a substructure is [21]

$$\omega_1 = 7.14 \frac{N_s}{a^2} \sqrt{\frac{D}{m}} \tag{26}$$

It follows that the impedance matrix $\mathbf{Z}_{\mathrm{rr}}^{(s)}$ of the typical substructure shown in Figure 2 is positive definite for all values of $\sigma^2$ satisfying

$$\sigma^2 < \left( 7.14 \frac{N_s}{a^2} \sqrt{\frac{D}{m}} \right)^2 \tag{27}$$

In most shifted eigenvalue and forced frequency response problems, $\sigma$ is typically related to or described in terms of a natural circular frequency of the mechanical system of interest. Hence, for the square plate considered here, inequality (27) can be re-written as

$$\omega_{rn}^2 < 50.97 \frac{N_s^2}{a^4} \frac{D}{m} \tag{28}$$

which in view of Equation (24) can also be written as

$$\frac{\pi^4}{a^4} \left( r^2 + n^2 \right)^2 \frac{D}{m} < 50.97 \frac{N_s^2}{a^4} \frac{D}{m} \tag{29}$$

or

$$N_s > 1.38 \left( r^2 + n^2 \right) \tag{30}$$

It follows that in practice, given a $\sigma^2$, the number of substructures $N_s$ can be increased—or equivalently, the size of the substructures can be decreased—to prevent $\mathbf{Z}_{\mathrm{rr}}^{(s)}$ from being singular

 

or very ill-conditioned. For the plate problem exemplified here, if $r = n = 20$, Equation (30) reveals that decomposing the plate shown in Figure 2 in 1104 substructures allows us to consider mass-shifting its global stiffness matrix by a real positive number of the order of the square of the natural circular frequency of its 400th mode, or constructing a global impedance matrix corresponding to this mode, while maintaining each local matrix $\mathbf{Z}_{rr}^{(s)}$ positive definite. This is a very encouraging result given that for a FE model with a million dof or more, the performance of the FETI-DP solver is optimal when the number of substructures is of the order of a few thousands.

In summary, for many $\sigma^2$ values of practical interest, the global impedance matrix $\mathbf{Z}$ may be indefinite, but the local substructures impedances $\mathbf{Z}_{rr}^{(s)}$ can be maintained positive definite by choosing appropriately the number of substructures.

### *3.2. On the type of the dual interface problem*

Recall that in the context of Equation (1), $\widetilde{\mathbf{K}}_{cc}^{*}$ (16) has the meaning of the impedance matrix obtained when each substructure is treated as a superelement whose nodes are the substructure corner nodes. It follows that when the global impedance matrix $\mathbf{Z}$ (21) is indefinite, $\widetilde{\mathbf{K}}_{cc}^{*}$ is also indefinite. Hence, for undamped applications, even when the substructure impedance matrices $\mathbf{Z}_{rr}^{(s)}$ can be maintained positive definite by choosing appropriately the number of substructures $N_s$, the matrix $\left(\mathbf{F}_{I_{rr}} + \widetilde{\mathbf{F}}_{I_{rc}} \widetilde{\mathbf{K}}_{cc}^{*-1} \widetilde{\mathbf{F}}_{I_{rc}}^{T}\right)$ (15) will be in general indefinite. For damped applications, the matrices $\mathbf{F}_{I_{rr}}$, $\widetilde{\mathbf{F}}_{I_{rc}}$, and $\widetilde{\mathbf{Z}}_{cc}^{*}$ are complex-valued, and therefore the dual interface problem (15) is complex-valued. Therefore, in the context of Equation (1) or (2), a preconditioned generalized minimum residual (PGMRES) algorithm becomes more appropriate than a PCG algorithm for solving iteratively the dual interface problem (15).

### *3.3. Wave-based augmentation coarse modes*

Let $\mathbf{r}$ denote the residual associated with the iterative solution of the dual interface problem (15). From Equations (9)–(12) and Equation (15), it follows that

$$\mathbf{r} = \mathbf{d}_r - \widetilde{\mathbf{F}}_{I_{rc}} \widetilde{\mathbf{K}}_{cc}^{*-1} \tilde{\mathbf{f}}_c^{*} - \left(\mathbf{F}_{I_{rr}} + \widetilde{\mathbf{F}}_{I_{rc}} \widetilde{\mathbf{K}}_{cc}^{*-1} \widetilde{\mathbf{F}}_{I_{rc}}^{T}\right)\lambda = \sum_{s=1}^{N_s} \mathbf{B}_r^{(s)} \mathbf{u}_r^{(s)} \tag{31}$$

which shows that the residual $\mathbf{r}$ represents the jump of the iterate solution across the substructure interfaces. Hence, the FETI-DP method converges when the iterate $\mathbf{u}^n$ becomes continuous across all the substructure interfaces.

From Equations (12), (16), (15) and (11), it follows that at each iteration of a PGMRES algorithm applied to the solution of problem (15), FETI-DP forces the jump of the solution across the substructure interfaces to be orthogonal to the subspace represented by the matrix $\mathbf{Q}_b$. This feature is a strategy for designing an auxiliary coarse problem that, when $\mathbf{Q}_b$ is well chosen, accelerates the convergence of a DDM [14].

In this work, the search for a suitable matrix $\mathbf{Q}_b$ is driven by the following reasoning. Suppose that the space of traces on $\Gamma'$ of the solution of problem (1) is best approximated by a set of orthogonal vectors $\{\mathbf{v}_{j_E}\}_{j=1}^{N_v}$, where the subscript $E$ indicates that $\mathbf{v}_{j_E}$ is non-zero

 

only on edge $E \in \Gamma'$. Then, the residual $\mathbf{r}$ defined in Equation (31) can be approximated as

$$\mathbf{r} \approx \sum_{j=1}^{N_v} \alpha_j \mathbf{v}_{j_E} \tag{32}$$

where $\{\alpha_j\}_{j=1}^{N_v}$ is a set of $N_v$ coefficients. If each augmentation coarse mode is chosen as

$$\mathbf{q}_j = \mathbf{v}_{j_E}, \quad j = 1, \ldots, N_Q \tag{33}$$

Equation (12) simplifies to

$$\alpha_j = 0, \quad j = 1, \ldots, N_Q \tag{34}$$

In this case, Equation (34) implies that at each iteration of the PGMRES algorithm, the first $N_Q$ components of the residual $\mathbf{r}$ in the independent set $\{\mathbf{v}_{j_E}\}_{j=1}^{N_v}$ are zero. Hence, if a few vectors $\{\mathbf{v}_{j_E}\}_{j=1}^{N_Q}$, $N_Q \ll N_v$, that dominate expansion (32) can be found, choosing these vectors as coarse augmentation modes can be expected to accelerate the convergence of the iterative solution of the dual interface problem (15). It remains to exhibit such a set of orthogonal vectors $\mathbf{v}_{j_E}$ and construct a computationally efficient matrix $\mathbf{Q}_b$.

As stated in Section 1, the focus of this paper is on structural dynamics applications where $\mathbf{K}$ and $\mathbf{M}$ typically arise from the FE discretization of solids and/or plates and shells. A second-order elastodynamic problem is governed by Navier's displacement equations of motion

$$\mu \Delta u + (\Lambda + \mu) \nabla (\nabla \cdot u) + b = \rho \frac{\partial^2 u}{\partial t^2} \tag{35}$$

where $u \in \mathbb{R}^3$ denotes the displacement field of the elastodynamic system, $\Lambda$ and $\mu$ its Lamé moduli, $b \in \mathbb{R}^3$ its body forces, $\rho$ its density, and $t$ denotes time. If a harmonic motion is assumed, i.e. if

$$u(X, t) = v(X) \mathrm{e}^{-\mathrm{i}\omega t} \tag{36}$$

where $X \in \mathbb{R}^3$ denotes the spatial variables and $\omega$ denotes a circular frequency, the homogeneous form of Equation (35) becomes

$$\mu \Delta v + (\Lambda + \mu) \nabla (\nabla \cdot v) + \rho \omega^2 v = 0 \tag{37}$$

The free-space solutions of the above equation are

$$v = a_p \sin\big(k_p \theta \cdot X\big), \quad v = a_p \cos\big(k_p \theta \cdot X\big) \tag{38}$$

$$v = a_{s_1} \sin(k_s \theta \cdot X), \quad v = a_{s_1} \cos(k_s \theta \cdot X) \tag{39}$$

$$v = a_{s_2} \sin(k_s \theta \cdot X), \quad v = a_{s_2} \cos(k_s \theta \cdot X) \tag{40}$$

where $\theta \in \mathbb{R}^3$ is an arbitrary vector of unit length ($\|\theta\|_2 = 1$), $a_p \in \mathbb{R}^3$ is a vector that is parallel to $\theta$, $\big(a_{s_1}, a_{s_2}\big) \in \mathbb{R}^3 \times \mathbb{R}^3$ are two independent vectors in the plane orthogonal to $\theta$

$$k_p = \sqrt{\frac{\rho \omega^2}{\Lambda + 2\mu}} \quad \text{and} \quad k_s = \sqrt{\frac{\rho \omega^2}{\mu}} \tag{41}$$

 

The free-space solutions (38) are known as the elastic pressure or longitudinal waves, and the free-space solutions (39) and (40) are known as the elastic shear or transverse waves.

Consider next the following fourth-order PDE associated with a given elastic body

$$\Delta^2 u - \frac{m}{D}\omega^2 u = 0 \tag{42}$$

where all variables have the same meaning as before. The reader can check that the free-space solutions (38)–(40) with

$$k_p = k_s = \sqrt[4]{\frac{m}{D}\omega^2} \tag{43}$$

are also free-space solutions of Equation (42). The PDE (42) can model the harmonic transverse motion of a plate. In this case, $u$ is a scalar representing the transverse displacement field. However, for the purpose of constructing an augmented coarse problem for the FETI-DP method, and only for this purpose, it is assumed here that when $u \in \mathbb{R}^3$, Equation (42) can model the harmonic motion of a shell in all three dimensions.

Hence, a general solution of either Equation (37) or (42) can be written as follows:

$$\begin{aligned} v = &\sum_{j=1}^{\infty} \left\{ a_{p_j} \left( c_{0_j} \sin\left(k_p \theta_j \cdot X\right) + c_{1_j} \cos\left(k_p \theta_j \cdot X\right) \right) \right\} \\ &+ \sum_{j=1}^{\infty} \left\{ a_{s_{1_j}} \left( c_{2_j} \sin\left(k_s \theta_j \cdot X\right) + c_{3_j} \cos\left(k_s \theta_j \cdot X\right) \right) \right\} \\ &+ \sum_{j=1}^{\infty} \left\{ a_{s_{2_j}} \left( c_{4_j} \sin\left(k_s \theta_j \cdot X\right) + c_{5_j} \cos\left(k_s \theta_j \cdot X\right) \right) \right\} \end{aligned} \tag{44}$$

where $\theta_j \in \mathbb{R}^3$ is an arbitrary vector of unit length defining the direction of propagation of an elastic pressure or shear wave, $c_{0_j}$, $c_{1_j}$, $c_{2_j}$, $c_{3_j}$, $c_{4_j}$, and $c_{5_j}$ are real coefficients, and $k_p$ and $k_s$ are given by Equation (41) for a second-order elastodynamic problem and by Equation (43) for a fourth-order plate or shell dynamic problem. From Equations (44) and (33), it follows that one choice for the desired matrix $\mathbf{Q}_{\mathrm{b}}$ is a matrix composed of blocks of six columns, where the columns of each block are associated with one direction of propagation $\theta_j$ and one edge $E$ of the mesh partition. This choice can be expressed as follows:

$$\mathbf{q}_{\mathrm{b}_l} \begin{bmatrix} 3(m-1)+1 \\ 3(m-1)+2 \\ 3(m-1)+3 \end{bmatrix} = a_{p_j} \sin\left(k_p \theta_j \cdot X_m\right), \quad \mathbf{q}_{\mathrm{b}_{l+1}} \begin{bmatrix} 3(m-1)+1 \\ 3(m-1)+2 \\ 3(m-1)+3 \end{bmatrix} = a_{p_j} \cos\left(k_p \theta_j \cdot X_m\right)$$

$$\mathbf{q}_{\mathrm{b}_{l+2}} \begin{bmatrix} 3(m-1)+1 \\ 3(m-1)+2 \\ 3(m-1)+3 \end{bmatrix} = a_{s_{1_j}} \sin\left(k_s \theta_j \cdot X_m\right), \quad \mathbf{q}_{\mathrm{b}_{l+3}} \begin{bmatrix} 3(m-1)+1 \\ 3(m-1)+2 \\ 3(m-1)+3 \end{bmatrix} = a_{s_{1_j}} \cos\left(k_s \theta_j \cdot X_m\right)$$

 

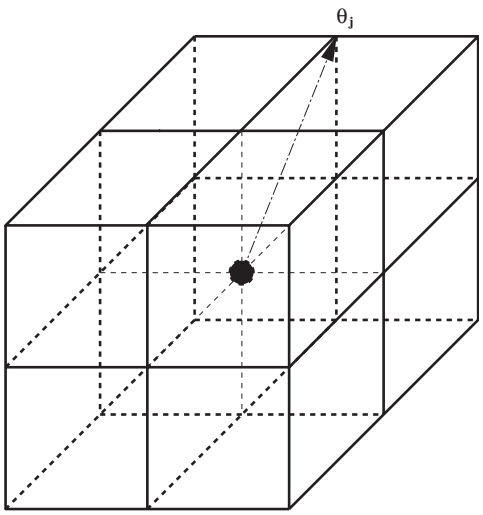


Figure 3. Generation of the directions of wave propagation ($n_c = 3$).

$$\mathbf{q}_{b_{l+4}}\begin{bmatrix}3(m-1)+1\\3(m-1)+2\\3(m-1)+3\end{bmatrix} = a_{s_{2j}}\sin\left(k_s\theta_j\cdot X_m\right), \quad \mathbf{q}_{b_{l+5}}\begin{bmatrix}3(m-1)+1\\3(m-1)+2\\3(m-1)+3\end{bmatrix} = a_{s_{2j}}\cos\left(k_s\theta_j\cdot X_m\right)$$

$$l = 6(j-1)+1, \quad m = 1,\ldots,N_I - N_c \tag{45}$$

where $\mathbf{q}_b[3(m-1)+1]$ designates the entry of $\mathbf{q}_b$ associated with the dof in the $x$-direction attached to the $m$th node on an edge $E \in \Gamma'$, $\mathbf{q}_b[3(m-1)+2]$ designates the entry associated with the dof along the $y$-direction, $\mathbf{q}_b[3(m-1)+3]$ designates the entry associated with the dof along the $z$-direction, and $X_m \in \mathbb{R}^3$ denotes the co-ordinates of this $m$th node. Hence, if $N_E$ denotes the number of edges of the mesh partition, and $N_\theta$ the number of considered directions of wave propagation, the total number of augmentation coarse modes is given in general by

$$N_Q = 6N_E N_\theta \tag{46}$$

To these modes can be added the edge-based translational (18) and/or rotational rigid body modes as these are free-space solutions of Equation (37) when $\omega = 0$.

In this paper, the directions $\theta_j$ are generated as follows. A generic cube is discretized into $n_c \times n_c \times n_c$ points. A direction $\theta_j$ is defined by connecting the centre of the cube to a point lying on a face of the cube (Figure 3). Since each direction $\theta_j$ is used to define both a cosine and a sine mode, only one direction is retained for each pair of opposite directions. This results in a total number of directions

$$N_\theta = \frac{\left(n_c^3 - (n_c-2)^3\right)}{2} \tag{47}$$

 

Hence, for a specified $N_\theta$, $n_c$ is chosen so that $N_\theta$ is as close as possible to the value given by the above equation.

### *3.4. Filtering the coarse space*

There are at least three mechanisms that can cause the matrix $\mathbf{Q}_b$ described in Section 3.3 to be rank deficient:

1. If a direction $\theta_j$ turns out to be perpendicular to an edge $E \in \Gamma'$, $\theta_j \cdot X_m$ becomes constant for all $X_m \in E$, the rank of the six-column block of $\mathbf{Q}_b$ associated with the edge $E$ and the direction $\theta_j$ becomes equal to three, and therefore $\mathbf{Q}_b$ becomes rank deficient.
2. Similarly, if a direction $\theta_j$ turns out to be perpendicular to all vectors $X_m \in E$, $\theta_j \cdot X_m = 0$, the rank of the six-column block of $\mathbf{Q}_b$ associated with $E$ and $\theta_j$ becomes equal to three, and therefore $\mathbf{Q}_b$ becomes rank deficient.
3. In the appendix, it is shown that an interplay between a low mesh resolution and $N_\theta$ can also cause $\mathbf{Q}_b$ to become rank deficient.

From Equation (12) or the definition of $\widetilde{\mathbf{K}}^*_{cc}$ given in the fifth of Equations (16), it follows that whenever $\mathbf{Q}_b$ does not have full column rank, $\widetilde{\mathbf{K}}^*_{cc}$ becomes singular. Singular coarse problems can be solved by a number of different techniques among which is the drop-tolerance-based direct method described in Reference [22]. However, preventing $\mathbf{Q}_b$ from being rank deficient—and therefore preventing $\widetilde{\mathbf{K}}^*_{cc}$ from being singular—is desirable as this improves the computational efficiency as well as the robustness of the solution of the coarse problem (17), and therefore enhances the efficiency and robustness of the overall solution method.

Let $\varepsilon_{QR}$ denote a small tolerance value. The following describes a simple procedure for filtering the matrix of augmentation coarse modes $\mathbf{Q}_b$ and transforming it into a matrix $\mathbf{Q}^*_b$ that has full column rank:

1. Perform the **QR** factorization [23] of $\mathbf{Q}_b$.
2. Construct $\mathbf{Q}^*_b$ as the union of the columns $\mathbf{q}_j$ of $\mathbf{Q}_b$ for which $\mathbf{R}_{jj} > \varepsilon_{QR}$.

The following observations are worth noting:

1. Since each column of $\mathbf{Q}_b$ has non-zero entries only for the dof associated with a corresponding edge $E$, the **QR** factorization of $\mathbf{Q}_b$ entails only *local* computations that can be performed on an edge-by-edge basis. Hence, these computations are amenable to an efficient parallelization.
2. A too small value of $\varepsilon_{QR}$ can result in a matrix $\mathbf{Q}^*_b$ that is still rank deficient, thereby defeating the purpose of the filtering procedure. On the other hand, a too large value of $\varepsilon_{QR}$ can only cause an excessive filtering. Since the columns of $\mathbf{Q}_b$ serve only the purpose of defining *optional* constraints aimed at accelerating the convergence of the iterative DDM (see Equation (12)), it follows that this DDM is better served by setting $\varepsilon_{QR}$ to a value that is sufficiently large to prevent $\mathbf{Q}^*_b$ from being rank deficient, even if such a tolerance can cause occasionally an excessive filtering of the matrix $\mathbf{Q}_b$.

*Remark*

From Section 3.3 (and in particular (46)) it follows that given a mesh partition characterized by a number of substructures $N_s$, fixing the number of wave directions $N_\theta$ determines the

 

size of the coarse problem (17) and therefore fixes in principle the cost of an iteration of the extension of the FETI-DP method developed here, independently of the value of the shift $\sigma$. However, when the tolerance $\varepsilon_{QR}$ is fixed, $N_s$ and $N_\theta$ are kept constant, but $\sigma$ is varied; the filtering procedure described above can result in a size of the coarse problem (17) that varies with $\sigma$. Essentially, this is because $k_p$, $k_s$—and therefore the columns of $Q_\mathrm{b}$ and the matrix $\widetilde{\mathbf{K}}^*_{\mathrm{cc}}$—depend on $\sigma$ (see Equations (41) and (43) with $\sigma = \omega$). For a fixed value of $\varepsilon_{QR}$, a higher value of $\sigma$ typically results in filtering out fewer columns of $Q_\mathrm{b}$ and therefore in generating a larger coarse problem (17) than a lower value of $\sigma$. For this reason, in practice, the cost of one iteration of the extension of the FETI-DP solver developed in this paper can be expected to vary with $\sigma$ even when the mesh partition ($N_s$) and the number of wave directions ($N_\theta$) are fixed.

### *3.5. Tailoring the Dirichlet and lumped preconditioners*

$\mathbf{M}^{(s)}_{\mathrm{rr}}$ is a mass matrix; hence, in three dimensions and at the element level, this matrix is proportional to $h^3$. On the other hand, $\mathbf{K}^{(s)}_{\mathrm{rr}}$ is a stiffness matrix; in three dimensions and at the element level, it is proportional to $h$ for second-order elasticity problems, and to $1/h^2$ for fourth-order plate and shell problems. It follows that for a sufficiently fine mesh, $\mathbf{Z}^{(s)}_{\mathrm{rr}}$ is dominated by $\mathbf{K}^{(s)}_{\mathrm{rr}}$. These observations suggest that the local matrices $\mathbf{Z}^{(s)}_{\mathrm{rr}}$ can be preconditioned by Dirichlet and lumped constructs (see Section 2.4) that are based on the $\mathbf{K}^{(s)}_{\mathrm{rr}}$ stiffness matrices rather than the $\mathbf{Z}^{(s)}_{\mathrm{rr}}$ impedance matrices. This results in real-valued $\overline{\mathbf{F}}^{D^{-1}}_{I_{\mathrm{rr}}}$ and $\overline{\mathbf{F}}^{L^{-1}}_{I_{\mathrm{rr}}}$ local preconditioners and therefore reduces storage cost when the original problem is complex-valued.

When Rayleigh damping is used, the substructure damping matrices can be written as

$$\mathbf{D}^{(s)}_{\mathrm{rr}} = c_K \mathbf{K}^{(s)}_{\mathrm{rr}} + c_M \mathbf{M}^{(s)}_{\mathrm{rr}} \tag{48}$$

where $c_K$ and $c_M$ are two real constants. In this case, the same reasoning as above can be invoked to justify preconditioning the local matrices $\mathbf{Z}^{D^{(s)}}_{\mathrm{rr}}$ by simpler Dirichlet and lumped constructs that are based on $(1 + \mathrm{i}\sigma c_K)\mathbf{K}^{(s)}_{\mathrm{rr}}$ rather than $\mathbf{Z}^{D^{(s)}}_{\mathrm{rr}}$.

Finally, it is pointed out that the *ad hoc* reasoning outlined above can be mathematically justified, at least in the context of the scalar Helmholtz equation which is closely related to the vector elastodynamic equation (35) (for example, see References [24, 25] and the references cited therein).

### *3.6. A substructure-based preconditioned GMRES solver with an auxiliary coarse problem*

In summary, the FETI-DP method is extended here to address the solution of problems of the form given in (1) or (2) by

1. replacing the CG interface solver by the GMRES interface solver;
2. adapting the Dirichlet and lumped preconditioners as explained in Section (3.5);
3. choosing as augmentation coarse modes the wave propagation modes derived in Section (3.3).

Because the wave propagation modes (45) are reminiscent of the plane wave modes $\mathrm{e}^{\mathrm{i}k\theta_j^{\mathrm{T}} X_\mathrm{b}}$ that characterize the FETI-H method [19] ($X_\mathrm{b}$ denotes here the co-ordinates of a node on $\Gamma$), the extension of the FETI-DP method defined above is named here the FETI-DPH method.

 

## 4. PARALLEL IMPLEMENTATION

All computational steps of the FETI-DPH method described in this paper, except the solution of the coarse problem (17), can be carried out on a substructure-by-substructure basis. Hence, these computations are trivially parallelized by assigning one or several substructures to each processor. In this work, all substructure problems are solved by a sparse direct method. If the given parallel processor consists of a network of shared memory parallel boxes (or boards), the coarse problem is duplicated in each box. Otherwise, it is duplicated in each processor. In all cases, this coarse problem is solved by a *sequential* sparse direct method. As long as the size of the coarse problem is small compared to the size of the global problem, and the target number of processors $N_p$ is also small, this serial step should not affect the overall performance of the parallel implementation of the FETI-DPH solver adopted in this work. Otherwise, it can degrade the overall parallel performance (see next section for details).

*Remark*
In Reference [26], a parallel distributed algorithm was proposed for solving FETI coarse problems on massively parallel systems. As in this paper, this algorithm assumes that the matrix governing the coarse problem is duplicated in each processor. It factors this matrix on every processor, computes in parallel its inverse and distributes it across the processors, and transforms all forward and backward solvers arising from the solution of coarse problems into parallel matrix–vector products. In Reference [26], this algorithm was shown to deliver a good performance and an excellent parallel scalability for up to 1000 processors, as long as each processor is mapped onto one substructure only. Unfortunately, this algorithm is computationally inefficient when more than one substructure is assigned to a single processor—that is, when the number of substructures is larger than the number of processors. As such, it is not a better alternative to a sequential sparse direct method on small systems with a few processors, unless the problem to be solved is sufficiently small to warrant decomposing it into a few substructures.

## 5. PERFORMANCE ASSESSMENT

In this section, the FETI-DPH method is applied to the solution of various problems of the form given in (1) or (2) and associated with the vibration analyses of a cylinder head and a car wheel. The cylinder head is represented by a FE model constructed with 8-noded brick and 3-noded shell elements (Figure 4). The car wheel is modelled by 3-noded triangular shell elements (Figure 5). All right sides $\mathbf{f}$ (see Equations (1) and (2)) are generated from a distributed load. Whenever either structure is assumed to be passively damped, Equation (48) is used to construct the FE damping matrix $D$, and the coefficients $c_K$ and $c_M$ are determined by requiring that the critical damping ratio of the first 5 modes of the structure be equal in a least-squares sense to a specified value, $\xi$. In all cases, the shift is chosen so that $\sigma^2 = \omega^2 = 4\pi^2 f^2$, where $\omega^2$ is the square of a (possibly natural) circular frequency of the structure, and $f$ is the corresponding frequency in Hz. As stated in the introduction of this paper, such problems arise, for example, in the FE simulation of the forced response of a structure to a periodic excitation characterized by the frequency $f$, or during the eigenanalysis of a structure by an inverse shifted method.

 

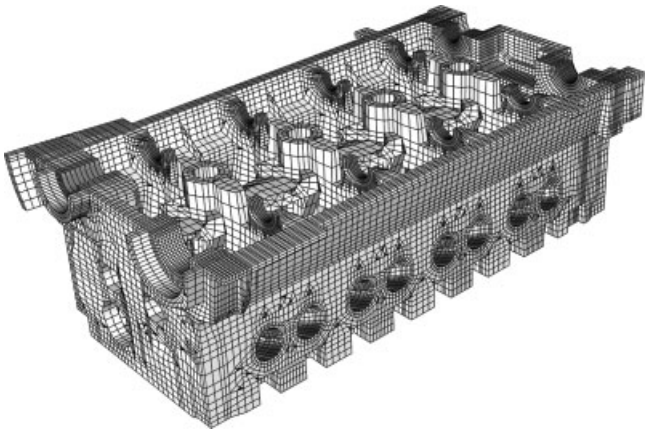

Figure 4. Finite element model of a cylinder head.

All computations are performed in double-precision arithmetic on a Silicon Graphics Origin 3200 computer equipped with 40 R12 000 400 MHz processors. This parallel system consists of 5 'boxes' of 8 processors each. On each box, the 8 processors share 8 Gigabytes of real memory. The 5 boxes are interconnected by a Brocade Silkwork 2400 switch.

As coded, the FETI-DPH solver relies on MPI for interprocessor communication and allows the number of substructures, $N_s$, to be different from the number of processors, $N_p$. In this work, the filtering tolerance is set to

$$\varepsilon_{QR} = 10^{-2} \tag{49}$$

and the convergence of this iterative solver is declared when the relative residual satisfies

$$RE^n = \frac{\left\| (\mathbf{K} - \sigma^2 \mathbf{M} + \mathrm{i}\sigma \mathbf{D})\mathbf{u}^n - \mathbf{f} \right\|_2}{\|\mathbf{f}\|_2} \leqslant 10^{-6} \tag{50}$$

if the structure is damped, and

$$RE^n = \frac{\left\| (\mathbf{K} - \sigma^2 \mathbf{M})\mathbf{u}^n - \mathbf{f} \right\|_2}{\|\mathbf{f}\|_2} \leqslant 10^{-6} \tag{51}$$

if it is undamped.

### *5.1. Cylinder head*

The cylinder head shown in Figure 4 is assumed to be attached to a rigid body at three different mounting locations in its lower part. Three different FE models are considered. Model CH-M1 contains 1055 3-noded shell elements, 11 587 8-noded solid elements, and 51 384 dof. Model CH-M2 is finer: it contains 4220 3-noded shell elements, 92 696 8-noded solid elements, and 326 847 dof. Model CH-M3 is obtained by further refining model CH-M2: it contains 16 880 3-noded shell elements, 741 568 8-noded brick elements, and 2 260 587 dof.

 

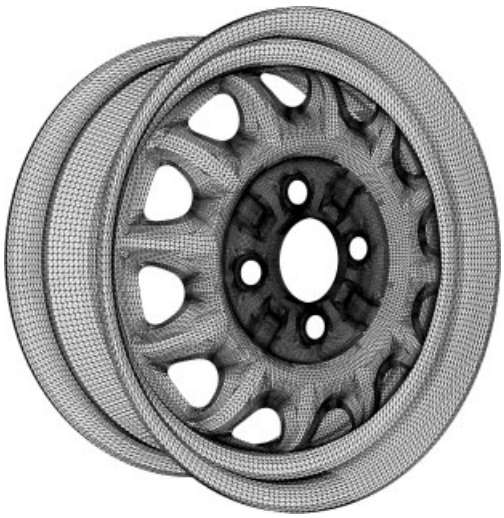

Figure 5. Finite element model of a car wheel.

In order to appreciate the magnitude of the various $\sigma$ values considered next for this problem, the spectrum of natural frequencies of this cylinder head is characterized in Table I using for this purpose the computational model CH-M2.

*5.1.1. Scalability studies for the undamped case.* Here, the cylinder head is assumed to be undamped. First, attention is focussed on model CH-M3 which is partitioned into 542, 789, 1040, and 1311 substructures. Four shift values ranging between $\sigma^2 = 3.95\text{e}+07$ and $\sigma^2 = 3.09\text{e}+10$ are considered. From the information reported in Table I, it follows that the smallest of these $\sigma^2$ values is close to the first eigenvalue of the pencil $(\mathbf{K}, \mathbf{M})$, and the largest of these values is greater than the 500th eigenvalue of the pencil $(\mathbf{K}, \mathbf{M})$. In all cases, the number of wave directions is set to $N_\theta = 3$, and the edge-based translational rigid body modes are added to the augmentation coarse modes. The performance results obtained on $N_p = 8$ processors are reported in Table II where $N_{\text{dof}}$ and $N_{\text{itr}}$ denote the total number of degrees of freedom and the number of iterations for convergence, respectively. For each considered shift value, the number of iterations of the FETI-DPH method is shown to be almost insensitive to the number of substructures, which suggests that the FETI-DPH solver is numerically scalable with respect to the number of substructures. Note that for a fixed number of wave directions $N_\theta$, the size of the coarse problem (17) increases with the number of substructures $N_s$. For this two-million-plus dof model, in most cases, the optimal value of $N_s$ appears to be somewhere between $N_s = 789$ and $N_s = 1040$, and the lumped preconditioner is reported to perform almost as well if not better than the Dirichlet preconditioner CPU-wise.

The optimal number of substructures for model CH-M1 turns out to be around $N_s = 45$, and that for CH-M2 turns out to be around $N_s = 300$. Table III reports the performance results obtained on $N_p = 8$ processors for the FETI-DPH solver applied to these models using their nearly optimal number of substructures. Again, these results show that in all cases, the lumped preconditioner performs as well as if not better CPU-wise than the Dirichlet preconditioner.

 

Table I. Partial spectrum of the pencil $(\mathbf{K}, \mathbf{M})$ (cylinder head).

| Mode number | Eigenvalue $(\omega^2)$ | Frequency $(f)$ (Hz) |
|---|---|---|
| 1 | 3.53e + 07 | 9.46e + 02 |
| 100 | 5.02e + 09 | 1.13e + 04 |
| 200 | 1.10e + 10 | 1.67e + 04 |
| 300 | 1.70e + 10 | 2.07e + 04 |
| 400 | 2.42e + 10 | 2.47e + 04 |
| 500 | 3.03e + 10 | 2.77e + 04 |
| 600 | 3.72e + 10 | 3.07e + 04 |
| 700 | 4.41e + 10 | 3.34e + 04 |
| 800 | 5.12e + 10 | 3.60e + 04 |
| 900 | 5.82e + 10 | 3.84e + 04 |
| 1000 | 6.55e + 10 | 4.07e + 04 |

Table II. Undamped cylinder head model CH-M3: $N_{\text{dof}} = 2\,260\,587$—$N_\theta = 3$ (+ the three translational rigid body modes)—$N_p = 8$.

| Frequency shift (Hz) | Shift $\sigma^2$ | $N_s$ | $N_{\text{itr}}$ (Lumped) | CPU (Lumped) (s) | $N_{\text{itr}}$ (Dirichlet) | CPU (Dirichlet) (s) |
|---|---|---|---|---|---|---|
| | | 542 | 89 | 746 | 60 | 848 |
| 1.0e + 03 | 3.95e + 07 | 789 | 70 | 528 | 46 | 547 |
| | | 1040 | 64 | 462 | 49 | 514 |
| | | 1311 | 63 | 459 | 46 | 512 |
| | | 542 | 204 | 1549 | 165 | 1778 |
| 1.70e + 04 | 1.14e + 10 | 789 | 171 | 1227 | 135 | 1274 |
| | | 1040 | 164 | 1195 | 130 | 1241 |
| | | 1311 | 168 | 1268 | 138 | 1355 |
| | | 542 | 218 | 1790 | 181 | 1955 |
| 2.10e + 04 | 1.74e + 10 | 789 | 182 | 1326 | 148 | 1436 |
| | | 1040 | 173 | 1288 | 143 | 1358 |
| | | 1311 | 180 | 1467 | 149 | 1498 |
| | | 542 | 317 | 2403 | 262 | 3075 |
| 2.80e + 04 | 3.09e + 10 | 789 | 272 | 1960 | 225 | 2087 |
| | | 1040 | 263 | 2002 | 223 | 2095 |
| | | 1311 | 260 | 2817 | 230 | 2310 |

Model CH-M2 is roughly 7 times larger than model CH-M1, and model CH-M3 is roughly 7 times as large as model CH-M2. For each considered shift value, the FETI-DPH solver is reported to consume about 9 times more CPU for model CH-M2 than for model CH-M1, and also about 9 times more CPU for model CH-M3 than for model CH-M2. This demonstrates a good scalability of the performance of the FETI-DPH solver with respect to the problem size.

Next, attention is focused again on the large-scale model CH-M3, the number of substructures is fixed to $N_s = 789$, and the shift value is set to $\sigma^2 = 1.74\text{e} + 10$ ($f = 2.10\text{e} + 04$ Hz). The number of wave directions is set to $N_\theta = 3$ and the edge-based translational rigid body modes are added to the augmentation coarse modes, which generate a coarse problem with a size

 

Table III. Undamped cylinder head: $N_\theta = 3$ (+ the three translational rigid body modes)—$N_p = 8$.

| Frequency shift (Hz) | Shift $\sigma^2$ | $N_{\text{dof}}$ | $N_s$ | $N_{\text{itr}}$ lumped | CPU lumped (s) | $N_{\text{itr}}$ Dirichlet | CPU Dirichlet (s) |
|---|---|---|---|---|---|---|---|
| | | 51 384 | 45 | 139 | 16 | 123 | 19 |
| 1.70e + 04 | 1.14e + 10 | 326 847 | 300 | 137 | 143 | 119 | 146 |
| | | 2 260 587 | 1040 | 164 | 1195 | 130 | 1241 |
| | | 51 384 | 45 | 166 | 19 | 151 | 22 |
| 2.10e + 04 | 1.74e + 10 | 326 847 | 300 | 159 | 145 | 162 | 126 |
| | | 2 260 587 | 1040 | 173 | 1288 | 143 | 1358 |
| | | 51 384 | 45 | 250 | 26 | 233 | 31 |
| 2.80e + 04 | 3.09e + 10 | 326 847 | 300 | 230 | 214 | 190 | 235 |
| | | 2 260 587 | 1040 | 263 | 2002 | 230 | 2310 |

$N_{\text{dof}}^{\text{coarse}} = 47\,226$. In this case, the performance of the FETI-DPH solver equipped with the lumped preconditioner is reported in Table IV for a number of processors varying between 4 and 40. The CPU performance on 4 processors is adopted as 'reference' performance because it takes 4 processors to meet the memory requirement of this problem. Excellent to good parallel speed-ups and efficiencies are achieved for $4 \leqslant N_p \leqslant 20$. In this range of number of processors, the amount of CPU time consumed by the sequential solution of the coarse problem varies between 16 and 53% of the total CPU time consumed by the parallel FETI-DPH solver. Once the ratio of sequential to parallel work reaches 53%, increasing the number of processors from 20 to 40 decreases the parallel efficiency of the FETI-DPH solver from 67 to 36%.

*5.1.2. Scalability studies for the damped case.* To illustrate the performance of the FETI-DPH solver for problems of the form given in (2), the cylinder head is next assumed to be damped. Model CH-M3 is considered again but with two different realistic damping levels described by $\xi = 1$ and 2%. As before, $N_\theta$ is set to 3 and the edge-based translational rigid body modes are added to the augmentation coarse modes. The performance results of the FETI-DPH solver equipped with the lumped preconditioner and obtained on $N_p = 16$ processors are reported in Table V. These results demonstrate the numerical scalability of the FETI-DPH method with respect to the number of substructures. Amazingly, they also reveal that the FETI-DPH solver converges faster for damped problems of the form given in (2) than for undamped problems of the form given in (1), and almost independently from the value of the shift $\sigma$. The reader is reminded that in the undamped case, the FETI-DPH solver operates in the real domain whereas in the damped case, it operates in the complex plane. This explains why, as can be expected, each iteration of FETI-DPH is slower in the presence of damping than in its absence. However, because of the faster convergence rate in the presence of damping, for a given problem, the FETI-DPH solver exhibits comparable CPU performances for the damped and undamped cases.

*5.1.3. Benchmark against a sparse solver.* Sparse direct solvers are popular in structural and solid mechanics, structural dynamics, and structural acoustics codes. They perform best on sequential computing platforms because they are not as well amenable to parallel processing

 

Table IV. Undamped cylinder head model CH-M3: $N_{\text{dof}} = 2\,260\,587$—$N_{\text{dof}}^{\text{coarse}} = 47\,226$—$\sigma^2 = 1.74\text{e}+10$ ($f = 2.10\text{e}+04$ Hz)—$N_s = 789$—Lumped preconditioner—$N_\theta = 3$ (+ the three translational rigid body modes).

| $N_p$ | CPU solution coarse problem (s) | CPU total (s) | Parallel speed-up overall | Parallel efficiency overall (%) |
|---|---|---|---|---|
| 4 | 358 | 2258 | Reference | Reference |
| 8 | 358 | 1326 | 6.8 | 85 |
| 12 | 358 | 918 | 8.8 | 82 |
| 16 | 358 | 707 | 12.8 | 80 |
| 20 | 358 | 675 | 13.4 | 67 |
| 24 | 358 | 650 | 13.9 | 58 |
| 28 | 358 | 641 | 14.1 | 50 |
| 32 | 358 | 639 | 14.1 | 44 |
| 40 | 358 | 635 | 14.2 | 36 |

as Krylov-based iterative solvers. Hence, the FETI-DPH solver is benchmarked here against a sparse direct solver in order to assess its intrinsic performance, and highlight its potential not only for parallel but also for serial production environments.

To this effect, the sparse direct solver considered in this work is the `BLK` solver developed at the Oak Ridge National Laboratories [27]; it is provided bundled with an optimal reordering scheme. This sparse solver is also used within FETI-DPH to solve the local substructure problems (9), their preconditioned versions, and every occurrence of the coarse problem (17). The CH-M2 model is chosen to generate the benchmark problem because it is a medium-scale finite element model. Small-scale models tend to favour sparse solvers. Large-scale models tend to favour iterative solvers, particularly from a memory viewpoint. The damping level is set to $\xi = 1\%$, and the shift parameter is set to $\sigma = 1.32\text{e}+05$ ($f = 2.10\text{e}+04$ Hz). The performance results obtained on a single processor are reported in Table VI. For this problem, the FETI-DPH solver equipped with the lumped preconditioner is reported to be 6 times faster than the `BLK` sparse solver. However, it is only 1.8 times more memory lean.

### 5.2. Car wheel

The car wheel shown in Figure 5 is assumed to be mounted at its centre on a testing equipment. Three different FE models are constructed using 3-noded shell elements. The first one, model CW-M1, contains 19 616 elements and 59 898 dof. The second one, model CW-M2, is finer: it contains 78 464 elements and 235 614 dof. The third model, CW-M3, is the finest with 313 856 elements and 936 102 dof.

Again, in order to appreciate the magnitude of the various $\sigma$ values considered next for this car wheel problem, the spectrum of its natural frequencies is characterized in Table VII using for this purpose the FE model CW-M2.

*5.2.1. Scalability studies for the undamped case.* Here, the car wheel is assumed to be undamped. First, attention is focused on model CW-M3 which is partitioned into 206, 359, and 461 substructures. Three shift values, namely $\sigma^2 = 1.00\text{e}+06$, $3.00\text{e}+09$, and $9.48\text{e}+09$ are considered. The first of these $\sigma^2$ values is close to the third lowest eigenvalue of the pencil

 

Table V. Damped cylinder head model CH-M3: $N_{\text{dof}} = 2\,260\,587$—Lumped preconditioner—$N_\theta = 3$ (+ the three translational rigid body modes)—$N_p = 16$.

| Frequency shift (Hz) | Shift $\sigma$ | Critical damping ratio $\xi$ (%) | $N_s$ | $N_{\text{itr}}$ | CPU (s) |
|---|---|---|---|---|---|
| | | | 542 | 204 | 734 |
| | | 0 | 789 | 171 | 615 |
| | | | 1040 | 164 | 677 |
| | | | 542 | 73 | 1015 |
| 1.70e + 04 | 1.07e + 05 | 1 | 789 | 53 | 844 |
| | | | 1040 | 50 | 982 |
| | | | 542 | 67 | 975 |
| | | 2 | 789 | 48 | 809 |
| | | | 1040 | 45 | 955 |
| | | | 542 | 218 | 809 |
| | | 0 | 789 | 182 | 707 |
| | | | 1040 | 173 | 726 |
| | | | 542 | 70 | 1060 |
| 2.10e + 04 | 1.32e + 05 | 1 | 789 | 50 | 947 |
| | | | 1040 | 46 | 993 |
| | | | 542 | 65 | 1034 |
| | | 2 | 789 | 46 | 923 |
| | | | 1040 | 43 | 967 |
| | | | 542 | 317 | 1197 |
| | | 0 | 789 | 272 | 1059 |
| | | | 1040 | 263 | 1159 |
| | | | 542 | 66 | 1174 |
| 2.80e + 04 | 1.76e + 05 | 1 | 789 | 47 | 1058 |
| | | | 1040 | 45 | 1211 |
| | | | 542 | 63 | 1161 |
| | | 2 | 789 | 43 | 1030 |
| | | | 1040 | 41 | 1195 |

Table VI. Damped cylinder head model CH-M2: $N_{\text{dof}} = 326\,847$—$\xi = 1\%$—$\sigma = 1.32\text{e} + 05$ ($f = 2.10\text{e} + 04$ Hz)—$N_s = 300$—Lumped preconditioner—$N_\theta = 3$ (+ the three translational rigid body modes)—$N_p = 1$.

| Sparse solver memory (Gbytes) | FETI-DPH memory (Gbytes) | Sparse solver total CPU (s) | FETI-DPH $N_{\text{itr}}$ | FETI-DPH total CPU (s) |
|---|---|---|---|---|
| 3.9 | 2.2 | 3568 | 36 | 589 |

($\mathbf{K}, \mathbf{M}$), the second of them is close to the 200th, and the third of these shift values is in the neighbourhood of the 400th eigenvalue of the pencil ($\mathbf{K}, \mathbf{M}$). In all cases, the number of wave directions is set to $N_\theta = 4$, and the edge-based translational and rotational rigid body modes are added to the augmentation coarse modes. The performance results obtained on $N_p = 8$

 

Table VII. Partial spectrum of the pencil $(\mathbf{K}, \mathbf{M})$ (car wheel).

| Mode number | Eigenvalue $(\omega^2)$ | Frequency $(f)$ (Hz) |
|---|---|---|
| 1 | 7.66e + 05 | 1.39e + 02 |
| 100 | 1.04e + 09 | 5.13e + 03 |
| 200 | 2.97e + 09 | 8.67e + 03 |
| 300 | 5.75e + 09 | 1.21e + 04 |
| 400 | 9.46e + 09 | 1.55e + 04 |
| 500 | 1.29e + 10 | 1.81e + 04 |

Table VIII. Undamped car wheel model CW-M3: $N_{\text{dof}} = 936\,102$—$N_\theta = 4$ (+ the translational and rotational rigid body modes)—$N_p = 8$.

| Frequency shift (Hz) | Shift $\sigma^2$ | $N_s$ | $N_{\text{itr}}$ (Lumped) | CPU (Lumped) (s) | $N_{\text{itr}}$ (Dirichlet) | CPU (Dirichlet) (s) |
|---|---|---|---|---|---|---|
| | | 206 | 175 | 329 | 81 | 150 |
| 1.59e + 02 | 1.00e + 06 | 359 | 142 | 278 | 60 | 127 |
| | | 461 | 145 | 226 | 62 | 139 |
| | | 206 | 345 | 567 | 181 | 393 |
| 8.72e + 03 | 3.00e + 09 | 359 | 161 | 281 | 86 | 214 |
| | | 461 | 167 | 330 | 85 | 233 |
| | | 206 | 190 | 288 | 120 | 254 |
| 1.55e + 04 | 9.48e + 09 | 359 | 155 | 285 | 97 | 238 |
| | | 461 | 169 | 354 | 96 | 268 |

Table IX. Undamped car wheel: $N_\theta = 4$ (+ the translational and rotational rigid body modes)—$N_p = 8$.

| Frequency shift (Hz) | Shift $\sigma^2$ | $N_{\text{dof}}$ | $N_s$ | $N_{\text{itr}}$ lumped | CPU lumped (s) | $N_{\text{itr}}$ Dirichlet | CPU Dirichlet (s) |
|---|---|---|---|---|---|---|---|
| | | 59 898 | 75 | 36 | 7 | 19 | 6 |
| 1.59e + 02 | 1.00e + 06 | 235 614 | 128 | 78 | 33 | 34 | 24 |
| | | 936 102 | 359 | 142 | 185 | 60 | 127 |
| | | 59 898 | 75 | 56 | 19 | 50 | 18 |
| 1.55e + 04 | 9.48e + 09 | 235 614 | 128 | 98 | 57 | 75 | 52 |
| | | 936 102 | 359 | 155 | 285 | 97 | 238 |

processors are reported in Table VIII. For each considered shift value, the FETI-DPH method exhibits numerical scalability with respect to the number of substructures, even when equipped with the lumped preconditioner. The optimal number of substructures appears to be $N_s = 359$. In all cases, the Dirichlet preconditioner is reported to outperform the lumped one iteration-wise and CPU-wise.

The optimal number of substructures for model CW-M1 turns out to be around $N_s = 75$, and that for model CW-M2 turns out to be around $N_s = 128$. Table IX reports the performance results obtained on $N_p = 8$ processors for the FETI-DPH solver applied to these models using

 

Table X. Undamped car wheel model CW-M3: $N_{\text{dof}} = 936\,102$—$N_{\text{dof}}^{\text{coarse}} = 25\,803$—$\sigma^2 = 9.48\text{e} + 09$ ($f = 1.55\text{e} + 04$ Hz)—$N_s = 359$—Dirichlet preconditioner—$N_\theta = 4$ (+ the translational and rotational rigid body modes).

| $N_p$ | CPU solution coarse problem (s) | CPU total (s) | Parallel speed-up overall | Parallel efficiency overall (%) |
|---|---|---|---|---|
| 4 | 115 | 346 | Reference | Reference |
| 8 | 115 | 238 | 5.8 | 73 |
| 12 | 115 | 184 | 7.5 | 63 |
| 16 | 115 | 179 | 7.7 | 48 |
| 20 | 115 | 159 | 8.6 | 43 |
| 24 | 115 | 154 | 9.0 | 37 |

their nearly optimal number of substructures. These results show that in all cases, the Dirichlet preconditioner outperforms the lumped one. Model CW-M3 is roughly 4 times larger than model CW-M2 and 16 times larger than model CW-M1. For both considered shift values, the FETI-DPH solver equipped with the Dirichlet preconditioner is reported to consume for model CW-M3 about 5 times more CPU than for model CW-M2, and 13 times more CPU than for model CW-M1. This suggests that the performance of the FETI-DPH solver equipped with the Dirichlet preconditioner is scalable with respect to the problem size.

Next, attention is focused again on the large-scale model CW-M3, the number of substructures is fixed to $N_s = 359$, and the shift value is set to $\sigma^2 = 9.48\text{e} + 09$ ($f = 1.55\text{e} + 04$ Hz). The number of wave directions is set to $N_\theta = 4$ and the edge-based translational and rotational rigid body modes are added to the augmentation coarse modes. This generates a coarse problem with a size $N_{\text{dof}}^{\text{coarse}} = 25\,803$. In this case, the performance of the FETI-DPH solver equipped with the Dirichlet preconditioner is reported in Table X for a number of processors varying between 4 and 24. Good parallel speed-ups and efficiencies are achieved for $4 \leqslant N_p \leqslant 12$. In this range of number of processors, the amount of CPU time consumed by the sequential solution of the coarse problem varies between 33 and 63% of the total CPU time consumed by the parallel FETI-DPH solver. Once the ratio of sequential to parallel work exceeds 63%, increasing the number of processors from 12 to 24 decreases the parallel efficiency of the FETI-DPH solver from 63 to 37%.

*5.2.2. Scalability studies for the damped case.* Next, the car wheel is assumed to be damped. Model CW-M3 is considered again but with two different realistic damping levels described by $\xi = 1$ and 2%. As before, $N_\theta$ is set to 4 and the edge-based translational and rotational rigid body modes are added to the augmentation coarse modes. The performance results of the FETI-DPH solver equipped with the Dirichlet preconditioner and obtained on $N_p = 8$ processors are reported in Table XI. They are also contrasted with the performance results obtained in the undamped case. Again, the reader is reminded that in the damped case, the FETI-DPH solver operates in the complex plane; in the undamped case, it operates in the real domain and therefore is naturally faster per iteration. As in the case of the cylinder head problem, the tabulated performance results reveal a numerical scalability of the FETI-DPH method with respect to the number of substructures. They also suggest that (a) for damped problems of the form given in (2), the performance of FETI-DPH solver is independent of the value of the

 

Table XI. Damped car wheel model CW-M3: $N_{\text{dof}} = 936\,102$—Dirichlet preconditioner—$N_\theta = 4$ (+ the translational and rotational rigid body modes)—$N_p = 8$.

| Frequency shift (Hz) | Shift $\sigma$ | Critical damping ratio $\xi$ (%) | $N_s$ | $N_{\text{itr}}$ | CPU (s) |
|---|---|---|---|---|---|
| | | | 206 | 81 | 150 |
| | | 0 | 359 | 60 | 127 |
| | | | 461 | 62 | 139 |
| | | | 206 | 81 | 333 |
| 1.59e + 02 | 1.00e + 03 | 1 | 359 | 60 | 262 |
| | | | 461 | 62 | 289 |
| | | | 206 | 81 | 329 |
| | | 2 | 359 | 60 | 279 |
| | | | 461 | 62 | 291 |
| | | | 206 | 181 | 393 |
| | | 0 | 359 | 86 | 214 |
| | | | 461 | 85 | 233 |
| | | | 206 | 43 | 319 |
| 8.72e + 03 | 5.47e + 04 | 1 | 359 | 37 | 334 |
| | | | 461 | 38 | 379 |
| | | | 206 | 42 | 351 |
| | | 2 | 359 | 36 | 317 |
| | | | 461 | 38 | 366 |
| | | | 206 | 120 | 254 |
| | | 0 | 359 | 97 | 238 |
| | | | 461 | 96 | 268 |
| | | | 206 | 40 | 340 |
| 1.55e + 04 | 9.73e + 04 | 1 | 359 | 32 | 322 |
| | | | 461 | 35 | 388 |
| | | | 206 | 49 | 343 |
| | | 2 | 359 | 32 | 323 |
| | | | 461 | 34 | 386 |

shift $\sigma$, and (b) its convergence rate is better for higher values of the shift than for lower ones, in which case this convergence rate is also better than that for undamped problems.

*5.2.3. Benchmark against a sparse solver.* Finally, the FETI-DPH solver equipped with the Dirichlet preconditioner is benchmarked against the `BLK` sparse direct solver for the FE model CW-M3 and a damping level defined by $\xi = 1\%$. The shift parameter is set to $\sigma = 9.73\text{e} + 04$ ($f = 1.55\text{e} + 04$ Hz). The performance results obtained on a single processor are reported in Table XII. They show that for this shell problem, the FETI-DPH solver equipped with the Dirichlet preconditioner is twice as fast as the `BLK` sparse solver. However, it reduces the memory requirement of the `BLK` sparse solver by 15% only. This is partly because sparse direct solvers are not as memory greedy for shell problems as they are for three-dimensional solid problems.

 

Table XII. Damped car wheel model CW-M3: $N_{\text{dof}} = 936\,102$—$\xi = 1\%$—$\sigma = 9.73\text{e} + 04$ ($f = 1.55\text{e} + 04$ Hz)—$N_s = 359$—Dirichlet preconditioner—$N_\theta = 4$ (+ the translational and rotational rigid body modes)—$N_p = 1$.

| Sparse solver memory (Gbytes) | FETI-DPH memory (Gbytes) | Sparse solver total CPU (s) | FETI-DPH $N_{\text{itr}}$ | FETI-DPH total CPU (s) |
|---|---|---|---|---|
| 4.7 | 4.0 | 2176 | 40 | 1085 |

## 6. CONCLUSIONS

The domain decomposition-based FETI-DPH iterative solution method presented in this paper addresses a class of indefinite problems of the form $(\mathbf{K} - \sigma^2\mathbf{M})\mathbf{u} = \mathbf{f}$, and a class of complex problems of the form $(\mathbf{K} - \sigma^2\mathbf{M} + \mathrm{i}\sigma\mathbf{D})\mathbf{u} = \mathbf{f}$, where $\mathbf{K}$, $\mathbf{M}$, and $\mathbf{D}$ are three real symmetric matrices arising from the finite element discretization of solid and shell dynamic problems, i is the imaginary complex number, and $\sigma$ is a real positive number. This method is essentially an extension of the FETI-DP [5, 6] method that can be characterized as follows. The interface problem is solved by a PGMRES algorithm instead of a conjugate gradient algorithm. For second-order elastodynamic problems, the basic coarse problem is augmented with free-space solutions of Navier's homogeneous displacement equations of motion. These free-space solutions are also known as the elastic pressure (or longitudinal) and shear (or transverse) waves. For plate and shell dynamic problems, the basic FETI-DP coarse problem is augmented with free-space solutions of the fourth-order partial differential equation modelling the harmonic transverse motion of a plate. For the case of real-valued problems, local singularities (or resonances) are avoided by choosing a sufficiently fine mesh partition. Numerical studies performed for large-scale problems that are representative of a class of structural dynamics applications in the automotive industry suggest that the proposed FETI-DPH method is numerically scalable with respect to all of the problem size, substructure size, and number of substructures. They also reveal that this method can handle values of $\sigma^2$ that are large in comparison with the converged eigenvalues of the pencil $(\mathbf{K}, \mathbf{M})$. On a single processor, FETI-DPH is found to be 6 times faster than a good sparse direct solver when the finite element model contains essentially solid elements and about 300 000 dof, and twice as fast when it contains essentially shell elements and about 900 000 dof. A parallel implementation of FETI-DPH in which the solution of the coarse problem is however serialized delivers a good parallel efficiency for up to 28 processors in the first case, and 16 processors in the second case. However, if this implementation is to be executed efficiently on more processors, it requires first parallelizing the coarse problem solver.

## APPENDIX A

The objective of this appendix is to show that an interplay between a low mesh resolution and the number of wave directions $N_\theta$ can cause the matrix $\mathbf{Q}_{\text{b}}$ to become rank deficient. Hence, this interplay is one among several motivations for filtering the matrix of augmentation coarse modes $\mathbf{Q}_{\text{b}}$ as described in Section 3.4.

 

For simplicity, the following proposition considers the case of a two-dimensional problem, a uniform discretization characterized by a mesh size $h$, and an edge $E$ of the mesh partition that is aligned with the $x$-axis and begins at its origin. In this case

$$\theta_j = \begin{bmatrix} \cos\vartheta_j \\ \sin\vartheta_j \end{bmatrix}, \quad X_m = \begin{bmatrix} x_m \\ 0 \end{bmatrix} = \begin{bmatrix} mh \\ 0 \end{bmatrix}, \quad \theta_j \cdot X_m = x_m \cos\vartheta_j \tag{A1}$$

and Equations (45) become

$$\mathbf{q}_{\mathrm{b}_l} \begin{bmatrix} 2(m-1)+1 \\ 2(m-1)+2 \end{bmatrix} = a_{p_j} \sin\big(k_p x_m \cos\vartheta_j\big), \quad \mathbf{q}_{\mathrm{b}_{l+1}} \begin{bmatrix} 2(m-1)+1 \\ 2(m-1)+2 \end{bmatrix} = a_{p_j} \cos\big(k_p x_m \cos\vartheta_j\big)$$

$$\mathbf{q}_{\mathrm{b}_{l+2}} \begin{bmatrix} 2(m-1)+1 \\ 2(m-1)+2 \end{bmatrix} = a_{s_j} \sin\big(k_s x_m \cos\vartheta_j\big), \quad \mathbf{q}_{\mathrm{b}_{l+3}} \begin{bmatrix} 2(m-1)+1 \\ 2(m-1)+2 \end{bmatrix} = a_{s_j} \cos\big(k_s x_m \cos\vartheta_j\big)$$

$$l = 4(j-1)+1$$

$$m = 1, \ldots, N_I - N_{\mathrm{c}} \tag{A2}$$

*Proposition*
Let $k$ denote either a wave number $k_p$ associated with a pressure wave, or a wave number $k_s$ associated with a shear wave (see Equations (41)). If the augmentation coarse problem contains two directions $\theta_i$ and $\theta_j$ whose angles with the $x$-axis $\vartheta_i$ and $\vartheta_j$ satisfy

$$\cos\vartheta_i \pm \cos\vartheta_j = \frac{2n\pi}{kh} \tag{A3}$$

where $n$ is an integer, then

1. $\vartheta_i$ and $\vartheta_j$ satisfy

$$\cos(kx_m \cos\vartheta_i) = \cos\big(kx_m \cos\vartheta_j\big), \quad \forall X_m \in E \tag{A4}$$

2. The matrix $\mathbf{Q}_{\mathrm{b}}$ defined by Equations (A2) is rank deficient.

*Proof*
Since $E$ is aligned with the $x$-axis and begins at its origin, and the mesh is assumed to be uniform, then

$$\forall X_m \in E, \quad x_m = mh \tag{A5}$$

From Equations (A3) and (A5) it follows that:

$$\cos(kx_m \cos\vartheta_i) = \cos\left(kx_m \left(\frac{2n\pi}{kh} \mp \cos\vartheta_j\right)\right)$$

 

$$= \cos\left(\mp k x_m \cos\vartheta_j + x_m \frac{2n\pi}{h}\right)$$

$$= \cos\left(\mp k x_m \cos\vartheta_j + (mh)\frac{2n\pi}{h}\right)$$

$$= \cos\left(\mp k x_m \cos\vartheta_j + 2nm\pi\right)$$

Hence, $\forall X_m \in E$,

$$\cos(k x_m \cos\vartheta_i) = \cos\left(k x_m \cos\vartheta_j\right)$$

From Equation (A2) and the above result it follows that the matrix $\mathbf{Q}_\mathrm{b}$ has at least two identical columns and therefore is rank deficient. □

Since $|\cos\vartheta_i \pm \cos\vartheta_j| \leqslant 2$, the result stated in the above proposition is significant when $2\pi/kh \leqslant 2/n$—and, therefore, when the mesh resolution is less or equal to 2 elements per wavelength ($n = 1$)—and when the augmentation coarse problems contain two directions $\theta_i$ and $\theta_j$ for which $\cos\vartheta_i = -\cos\vartheta_j$ ($n = 0$).

ACKNOWLEDGEMENTS

This research was supported by the Sandia National Laboratories under Contract No. 31095. The first author also acknowledges the support by the Sandia National Laboratories under Contract No. 29341, and the second author also acknowledges partial support by the National Science Foundation under Grant No. DMS-0209297. Any opinions, findings, and conclusions or recommendations expressed in this material are those of the authors and do not necessarily reflect the views of the Sandia National Laboratories or the National Science Foundation.

REFERENCES

1. Hager WW. *Applied Numerical Linear Algebra*. Prentice-Hall: Englewood Cliffs, NJ, 1988.
2. Pavarino LF, Toselli A. *Recent Developments in Domain Decomposition Methods*. Springer: Berlin, 2002.
3. Cai XC, Widlund O. Domain decomposition algorithms for indefinite elliptic problems. *SIAM Journal on Scientific and Statistical Computing* 1992; **13**:243–258.
4. Xu J, Cai XC. A preconditioned GMRES method for nonsymmetric or indefinite problems. *Mathematics of Computation* 1992; **59**:311–319.
5. Farhat C, Lesoinne M, Pierson K. A scalable dual-primal domain decomposition method. *Numerical Linear Algebra with Applications* 2000; **7**:687–714.
6. Farhat C, Lesoinne M, LeTallec P, Pierson K, Rixen D. FETI-DP: a dual-primal unified FETI method—Part I: a faster alternative to the two-level FETI method. *International Journal for Numerical Methods in Engineering* 2001; **50**:1523–1544.
7. Farhat C. A Lagrange multiplier based divide and conquer finite element algorithm. *Journal of Computer and System Engineering* 1991; **2**:149–156.
8. Farhat C, Roux FX. A method of finite element tearing and interconnecting and its parallel solution algorithm. *International Journal for Numerical Methods in Engineering* 1991; **32**:1205–1227.
9. Farhat C, Roux FX. An unconventional domain decomposition method for an efficient parallel solution of large-scale finite element systems. *SIAM Journal on Scientific and Statistical Computing* 1992; **13**:379–396.
10. Farhat C, Mandel J, Roux FX. Optimal convergence properties of the FETI domain decomposition method. *Computer Methods in Applied Mechanics and Engineering* 1994; **115**:367–388.

 

11. Mandel J, Tezaur R. On the convergence of a dual-primal substructuring method. *Numerische Mathematik* 2001; **88**:543–558.
12. Klawonn A, Widlund OB, Dryja M. Dual-primal FETI methods for three-dimensional elliptic problems with heterogeneous coefficients. *SIAM Journal on Numerical Analysis* 2002; **40**:159–179.
13. Bhardwaj M, Pierson K, Reese G, Walsh T, Day D, Alvin K, Peery J, Farhat C, Lesoinne M. Salinas: a scalable software for high-performance structural and solid mechanics simulations. *Proceedings of the IEEE/ACM SC2002 Conference*, Baltimore, Maryland, 2002.
14. Farhat C, Chen PS, Risler F, Roux FX. A unified framework for accelerating the convergence of iterative substructuring methods with Lagrange multipliers. *International Journal for Numerical Methods in Engineering* 1998; **42**:257–288.
15. Farhat C, Mandel J. The two-level FETI method for static and dynamic plate problems—Part I: an optimal iterative solver for biharmonic systems. *Computer Methods in Applied Mechanics and Engineering* 1998; **155**:129–152.
16. Farhat C, Chen PS, Mandel J, Roux FX. The two-level FETI method—Part II: extension to shell problems, parallel implementation and performance results. *Computer Methods in Applied Mechanics and Engineering* 1998; **155**:153–180.
17. Lesoinne M. A FETI-DP corner selection algorithm for three-dimensional problems. *Proceedings of the 2002 Domain Decomposition Conference*, Cocoyoc, Mexico, 2002.
18. Rixen D, Farhat C. A simple and efficient extension of a class of substructure based preconditioners to heterogeneous structural mechanics problems. *International Journal for Numerical Methods in Engineering* 1999; **44**:489–516.
19. Farhat C, Macedo A, Lesoinne M. A two-level domain decomposition method for the iterative solution of high frequency exterior Helmholtz problems. *Numerische Mathematik* 2000; **85**:283–308.
20. Géradin M, Rixen D. *Mechanical Vibrations*. Wiley, Masson: New York, 1994.
21. Blevins RD. *Formulas for Natural Frequency and Mode Shape*. Robert E. Krieger Publishing Company: Malabar, Florida, 1984.
22. Farhat C, Géradin M. On the general solution by a direct method of a large-scale singular system of linear equations: application to the analysis of floating structures. *International Journal for Numerical Methods in Engineering* 1998; **41**:675–696.
23. Golub GH, Van Loan CF. *Matrix Computations*. Johns Hopkins: Baltimore, Maryland, 1983.
24. Yserentant H. Preconditioning indefinite discretization matrices. *Numerische Mathematik* 1988; **54**:719–734.
25. Klawonn A. Preconditioners for indefinite problems. *Ph.D. Thesis*, Westfalische, Wilhelms-Universitat, Munster, 1995.
26. Bhardwaj M, Day D, Farhat C, Lesoinne M, Pierson K, Rixen D. Application of the FETI method to ASCI problems: scalability results on one-thousand processors and discussion of highly heterogeneous problems. *International Journal for Numerical Methods in Engineering* 2000; **47**:513–536.
27. Ng E. Private communication.
28. Saad Y. *Iterative Methods for Sparse Linear Systems*. PWS Publishing Company: Boston, 1995.
29. Parlett BN. *The Symmetric Eigenvalue Problem*, Prentice Hall Series in Computational Mathematics. Prentice-Hall: Englewood Cliffs, NJ, 1980.


 